bioRxiv preprint doi: https://doi.org/10.1101/622266; this version posted April 29, 2019. The copyright holder for this preprint (which was not certified by peer review) is the author/funder, who has granted bioRxiv a license to display the preprint in perpetuity. It is made available under aCC-BY-NC-ND 4.0 International license.

Structural destabilization and chaperone-assisted proteasomal degradation of MLH1 as a mechanism for Lynch syndrome

Amanda B. Abildgaard[1], Amelie Stein[1,*], Katrine Schultz-Knudsen[1], Sofie V. Nielsen[1], Elena Papaleo[1,2], Amruta Shrikhande[3], Eva R. Hoffmann[3], Inge Bernstein[4], Anne-Marie Gerdes[5], Masanobu Takahashi[6], Chikashi Ishioka[6], Kresten Lindorff-Larsen[1,*] and Rasmus Hartmann-Petersen[1,*]

Running title: Degradation of cancer-linked MLH1 variants

Keywords: protein folding, misfolding, protein quality control, proteasome, HSP70

1: The Linderstrøm-Lang Centre, Department of Biology, University of Copenhagen, Ole Maaløes Vej 5, DK-2200 Copenhagen, Denmark.

2: Current address: Computational Biology Laboratory, Danish Cancer Society Research Center, Strandboulevarden 49, DK-2100 Copenhagen, Denmark.

3: Department of Cellular and Molecular Medicine, University of Copenhagen, Blegdamsvej 3B, DK-2200 Copenhagen, Denmark.

4: Department of Surgical Gastroenterology, Aalborg University Hospital, DK-9000 Ålborg, Denmark.

5: Department of Clinical Genetics, Rigshospitalet, Blegdamsvej 9, DK-2100 Copenhagen, Denmark.

6: Tohoku University Hospital, Tohoku University, Sendai, Japan.

*Corresponding authors: A.S. (amelie.stein@bio.ku.dk), K.L.-L. (lindorff@bio.ku.dk) and R.H.-P. (rhpetersen@bio.ku.dk).

bioRxiv preprint doi: https://doi.org/10.1101/622266; this version posted April 29, 2019. The copyright holder for this preprint (which was not certified by peer review) is the author/funder, who has granted bioRxiv a license to display the preprint in perpetuity. It is made available under aCC-BY-NC-ND 4.0 International license.

Abstract

A defective DNA mismatch repair (MMR) system leads to increased mutation rates and microsatellite instability. Accordingly, germline loss-of-function variants in any of the MMR components MSH2, MSH6, MLH1 and PMS2 are closely linked to the hereditary cancer predisposition disorder known as Lynch syndrome. As an early diagnosis increases survival, the identification of pathogenic variants in the MMR components is clinically important, but often complicated by many variants being of unknown pathogenic significance. Here we show that several disease-linked MLH1 protein variants are targeted by HSP70 for chaperone-assisted proteasomal degradation and are therefore present at reduced cellular amounts. In turn, this lower amount of MLH1 results in degradation of the MLH1-binding proteins PMS1 and PMS2. *In silico* saturation mutagenesis and computational prediction of the thermodynamic stability of all structurally-resolved MLH1 single-site missense variants revealed a correlation between the structural destabilization of MLH1, the reduced steady-state levels and loss-of-function. Accordingly, the thermodynamic stability predictions separate disease-linked *MLH1* missense mutations from benign *MLH1* variants, and therefore hold potential for classification of *MLH1* missense variants of unknown consequence, and hence for Lynch syndrome diagnostics.

bioRxiv preprint doi: https://doi.org/10.1101/622266; this version posted April 29, 2019. The copyright holder for this preprint (which was not certified by peer review) is the author/funder, who has granted bioRxiv a license to display the preprint in perpetuity. It is made available under aCC-BY-NC-ND 4.0 International license.

Introduction

The DNA mismatch repair (MMR) pathway corrects mismatched base pairs inserted during replication. The MutSα (MSH2-MSH6) heterodimer initiates repair by detecting the mismatch after which the MutLα (MLH1-PMS2) heterodimer promotes the process by generating a nick in the newly synthesized DNA strand, thereby stimulating downstream repair proteins (Jiricny, 2006; Jun et al., 2006). The MMR pathway is phylogenetically highly conserved, emphasizing its importance as a key DNA repair mechanism of the cell (Jiricny, 2013; Sachadyn, 2010). Loss of MMR activity causes genome instability, and can result in both sporadic and inherited cancer, such as Lynch Syndrome (LS) (OMIM: #609310), also known as hereditary nonpolyposis colorectal cancer (HNPCC). The predominant consequence of LS is colorectal cancer (CRC), making LS the underlying reason for around 4% of all CRC cases (Aarnio et al., 1999; Hampel et al., 2008; Moller et al., 2018; Sijmons and Hofstra, 2016; Thompson et al., 2014; Vasen et al., 1996; Vasen and de Vos Tot Nederveen Cappel WH, 2013). Importantly, the cumulative lifetime cancer risk varies considerably between patients and depends on the specific germline mutation in the genes encoding the key mismatch repair proteins MSH2, MSH6, MLH1, and PMS2 (Barrow et al., 2008; Dowty et al., 2013; Dunlop et al., 1997; Lynch et al., 2015; Peltomaki et al., 1993; Plaschke et al., 2004; Sijmons and Hofstra, 2016). The majority of LS cases result from *MLH1* and *MSH2* mutations (Peltomaki, 2016), many of which are missense mutations (Heinen, 2010; Palomaki et al., 2009; Peltomaki, 2016; Peltomaki and Vasen, 1997). Evidently, such missense mutations may cause loss-of-function by directly perturbing protein-protein interactions or ablating enzymatic activity. Many missense mutations, however, cause loss-of-function by inducing structural destabilization of the protein (Stein et al., 2019), which in turn may trigger protein misfolding and degradation by the ubiquitin-proteasome system (UPS) (Kampmeyer et al., 2017; Kriegenburg et al., 2014; Nielsen et al., 2014). As a result, the cellular amount of a

bioRxiv preprint doi: https://doi.org/10.1101/622266; this version posted April 29, 2019. The copyright holder for this preprint (which was not certified by peer review) is the author/funder, who has granted bioRxiv a license to display the preprint in perpetuity. It is made available under aCC-BY-NC-ND 4.0 International license.

missense protein may be reduced to an insufficient level, which can ultimately cause disease (Ahner et al., 2007; Casadio et al., 2011; Matreyek et al., 2018; Nielsen et al., 2017).

In this study, we investigated whether this is the case for LS-linked variants of the MLH1 protein. We determined cellular abundance for 69 missense variants, and show that several destabilized LS-linked MLH1 variants are targeted for chaperone-assisted proteasomal degradation and are therefore present at reduced cellular amounts. In turn, this lower amount of MLH1 results in degradation of the MLH1-binding proteins PMS1 and PMS2. *In silico* saturation mutagenesis and computational prediction of the thermodynamic stability of all possible MLH1 single site missense variants revealed a correlation between the structural destabilization of MLH1, reduced steady-state levels and the loss-of-function phenotype. Accordingly, the thermodynamic stability predictions accurately separate disease-linked *MLH1* missense mutations from benign *MLH1* variants, and therefore hold potential for classification of *MLH1* missense variants of unknown consequence, and hence for LS diagnostics. Further, by suggesting a mechanistic origin for many LS-causing *MLH1* missense variants our studies provide a starting point for development of novel therapies.

bioRxiv preprint doi: https://doi.org/10.1101/622266; this version posted April 29, 2019. The copyright holder for this preprint (which was not certified by peer review) is the author/funder, who has granted bioRxiv a license to display the preprint in perpetuity. It is made available under aCC-BY-NC-ND 4.0 International license.

Results

In silico saturation mutagenesis and thermodynamic stability predictions

Most missense proteins are less structurally stable than the wild-type protein (Tokuriki and Tawfik, 2009), and individual missense variants may thus lead to increased degradation and insufficient amounts of protein. To comprehensively assess this effect for MLH1, we performed energy calculations based on crystal structures of MLH1 to predict the consequences of missense mutations in *MLH1* on the thermodynamic stability of the MLH1 protein structure. Full-length human MLH1 is a 756 residue protein which forms two folded units, an N-terminal domain (residues 7-315) and a C-terminal domain (residues 502-756) (Mitchell et al., 2019) separated by a flexible and intrinsically disordered linker (Fig. 1A). Using the structures (Wu et al., 2015) of the two domains (PDB IDs 4P7A and 3RBN) (Fig. 1A), we performed *in silico* saturation mutagenesis, introducing all possible single site amino acid substitutions into the wild-type MLH1 sequence at the 564 structurally resolved residues. We then applied the FoldX energy function (Schymkowitz et al., 2005) to estimate the change in thermodynamic folding stability compared to the wild-type MLH1 protein (ΔΔG) (Fig. 1BC). Negative values indicate that mutations that are predicted to stabilize MLH1, while positive values indicate that the mutations may destabilize the MLH1 protein. Thus, those variants with ΔΔG predictions > 0 kcal/mol are expected to have a larger population of fully or partially unfolded structures that, in turn, may be prone to PQC-mediated degradation. Our saturation mutagenesis dataset comprises 19 (amino acids, excluding the wild-type residue) * 564 (residues resolved in the N- and C-terminal structures) = 10,716 different MLH1 variants, thus covering 75% of all possible missense variants in MLH1. We illustrate a subsection as a heat map in Fig. 1D (the entire dataset is included in the supplemental material, supplemental material file 1). The predictions reveal that 34% of the substitutions are expected to change the stability of MLH1 by less than 0.7 kcal/mol, which is

bioRxiv preprint doi: https://doi.org/10.1101/622266; this version posted April 29, 2019. The copyright holder for this preprint (which was not certified by peer review) is the author/funder, who has granted bioRxiv a license to display the preprint in perpetuity. It is made available under aCC-BY-NC-ND 4.0 International license.

the typical error of the predictions (Guerois et al., 2002) (Fig. 1E). A comparable fraction (32%) are, however, predicted cause a substantial destabilization (>2.5 kcal/mol) of the MLH1 protein (Fig. 1E).

Thermodynamic stability calculations predict severely reduced MLH1 steady-state levels

To test whether the *in silico* stability predictions are predictive of cellular stability, abundancy, and function, we selected 69 naturally occurring MLH1 missense variants with predicted ΔΔGs spanning from -1.6 to >15 kcal/mol (Table 1). We further ensured that the selected mutations were distributed throughout the *MLH1* gene, thus probing the entire structured parts of the MLH1 protein (Fig. 1A). Then, the variants were introduced into *MLH1*-negative HCT116 cells and analyzed by automated immunofluorescence microscopy using antibodies to MLH1.

As expected, wild-type MLH1 localized primarily to the nucleus (Fig. 2A). This localization pattern was also observed for all the MLH1 variants, and we did not detect any protein aggregates. We did, however, observe large variations in the fluorescence intensity, and consequently the steady-state protein levels, between the different MLH1 variants (Fig. 2A). To quantify these differences, we first excluded the non-transfected cells using the intensity in the non-transfected control. Then we measured the total intensity of the MLH1 fluorescence in each cell and normalized to the intensity for wild-type MLH1. This analysis revealed up to 12-fold difference in intensity between the variants showing sizable differences in abundance.

To examine whether these variations in cellular abundance is correlated with thermodynamic stability, we plotted the normalized values against the predicted structural stabilities (ΔΔGs). This analysis indeed reveals that those MLH1 variants that were predicted to be structurally destabilized (high ΔΔGs) also displayed reduced steady-state levels (Fig. 2B), indicating that the predicted structural destabilization and low steady-state MLH1 levels go hand in hand. Almost all (30 out of 31) variants with steady state > 75% have a ΔΔG < 3 kcal/mol, and similarly most (22/23) with ΔΔG

bioRxiv preprint doi: https://doi.org/10.1101/622266; this version posted April 29, 2019. The copyright holder for this preprint (which was not certified by peer review) is the author/funder, who has granted bioRxiv a license to display the preprint in perpetuity. It is made available under aCC-BY-NC-ND 4.0 International license.

< 3 kcal/mol have steady state levels <75%. A destabilization of 3 kcal/mol is relatively low threshold, but consistent with previous observations of other unrelated proteins (Bullock et al., 2000; Nielsen et al., 2017; Scheller et al., 2019). We believe that such low stability thresholds indicate that local unfolding (discussed below) plays an important role in the recognition and degradation of pathogenic variants.

Given that decreased levels of MLH1 protein could cause loss of MMR function we also examined whether cellular abundancy correlated with pathogenicity. Of the 69 variants that we studied, 29 are classified as pathogenic or likely pathogenic in the ClinVar database (Landrum et al., 2018), whereas 12 are (likely) benign, and 28 are variants of unknown significance. We found that all (likely) benign variants appeared stable and had steady-state levels >70% (Fig. 2B). Conversely, 18 out of the 29 pathogenic variants (62%) had steady-state levels < 70% of the (Fig. 2B), suggesting that protein destabilization is a common feature for many MLH1 variants linked to LS, and that predictions of stability might be useful for classifying variants.

Next, we analyzed how the measured steady-state levels and the stability predictions correlated with previously published *in vivo* functional data on MLH1 (Takahashi et al., 2007). In that study, MLH1 function was tested in a number of assays and ranked from 0 (no function) to 3 (full function) based on their dominant mutator effect (DME) when human MLH1 variants are expressed in yeast cells (Shimodaira et al., 1998). Our comparison revealed that variants with reduced steady-state levels and high risk of destabilization in general are less likely to be functional (Fig. 2CD), which again indicates that the reduced structural stability may be linked to the observed loss-of-function phenotype. For example, while 22/23 variants with DME=3 have steady state levels >70%, only five of the 23 variants with DME=0 have this high amount of protein. These functional differences are also reflected in the correlation between loss of stability ($\Delta\Delta G$) and function (Fig. 2D). In particular none of the fully functional proteins (DME=3) are predicted to be destabilized by more than 3 kcal/mol, whereas

bioRxiv preprint doi: https://doi.org/10.1101/622266; this version posted April 29, 2019. The copyright holder for this preprint (which was not certified by peer review) is the author/funder, who has granted bioRxiv a license to display the preprint in perpetuity. It is made available under aCC-BY-NC-ND 4.0 International license.

18/23 variants with DME=0 are predicted to be destabilized by at least this amount. The unstable and non-functional variants do not appear structurally clustered, but are found throughout both the N- and C-terminal domains of MLH1 (Fig. 2E). In contrast, the linker region is depleted in detrimental variants, while functional (Takahashi et al., 2007) and benign (Landrum et al., 2018) variants are found both in structured and unstructured regions (supplemental material, Fig. S1).

Proteasomal degradation causes reduced steady-state levels of destabilized MLH1 variants

Next, we analyzed why the steady-state levels of certain MLH1 variants were reduced. For this purpose, we carefully selected eight of the 69 missense MLH1 variants for further in-depth analyses (E23D, G67R, R100P, T117M, I219V, R265C, K618A, and R659P). As previously, these variants were chosen so the mutations were distributed across the *MLH1* gene, and to represent a broad range of predicted structural stabilities (ΔΔGs) as well as different pathogenicity annotations from the ClinVar database (Table 1).

The variants were transiently transfected into HCT116 cells. Indeed, six of the variants (G67R, R100P, T117M, R265C, K618A, R659P) displayed reduced steady-state levels, while wild type-like levels were observed for two variants (E23D, I219V), in agreement with the fluorescence-based observations (Fig. 3AB). Co-transfection with a GFP-expression vector revealed that this was not caused by differences between transfection efficiencies since the amount of GFP was unchanged (Fig. 3A).

Next, in order to investigate if the reduced MLH1 levels were caused by degradation, we monitored the amounts of MLH1 over time in cultures treated with the translation inhibitor cycloheximide (CHX). This revealed that those variants with reduced steady-state levels were indeed rapidly degraded (half-life between 3 and 12 hours), whereas wild-type MLH1 and the other variants appeared stable (estimated half-life >> 12 hours) (Fig. 3CD). Treating the cells with the proteasome-

bioRxiv preprint doi: https://doi.org/10.1101/622266; this version posted April 29, 2019. The copyright holder for this preprint (which was not certified by peer review) is the author/funder, who has granted bioRxiv a license to display the preprint in perpetuity. It is made available under aCC-BY-NC-ND 4.0 International license.

inhibitor bortezomib (BZ) significantly increased the steady-state levels of the unstable variants, whereas the levels of the wild-type and stable MLH1 variants were unaffected, indicating degradation by the proteasome (Fig. 3EF). Based on these results, we conclude that certain missense MLH1 variants are structurally destabilized, which in turn leads to proteasomal degradation and reduced steady-state protein levels, and a loss-of-function phenotype as scored by the DME.

PMS1 and PMS2 are destabilized when MLH1 is degraded

In order to carry out its role in MMR, it is essential that MLH1 associates with PMS2 to form the active MutLα complex (Li and Modrich, 1995; Raschle et al., 2002; Tomer et al., 2002). Additionally, MLH1 can bind the PMS1 protein and form the MutLβ complex, the function of which remains unknown (Cannavo et al., 2007; Kondo et al., 2001; Wu et al., 2003).

As typical for "orphan" proteins lacking their binding partners (McShane et al., 2016; Yanagitani et al., 2017), PMS2 has been found to be unstable in the absence of MLH1 (Hinrichsen et al., 2017; Lynch et al., 2015; Mohd et al., 2006; Perera and Bapat, 2008). To test the mechanism underlying this instability, we measured the stability of endogenous PMS1 and PMS2 in HCT116 cells with or without introducing wild-type MLH1. In cells treated with cycloheximide, the absence of MLH1 led to rapid degradation of both PMS1 and PMS2 ($t_{½}$ ~ 3-5 hours). However, when wild-type MLH1 was present, PMS1 and PMS2 were dramatically stabilized ($t_{½}$ ~ 12 hours) (Fig. 4AB). Treating untransfected HCT116 cells with bortezomib led to an increase in the amount of endogenous PMS1 and PMS2, showing that their degradation is proteasome-dependent (Fig. 4C). The stabilizing effect of MLH1 on PMS1 and PMS2 was also observed for the stable MLH1 variants (Fig. 4DE). Accordingly, we found that the MLH1 levels correlated with the PMS1 and PMS2 levels (Fig. 4F). Collectively, these results suggest that either there is not enough MLH1 variant in the cells to form complexes with PMS1/2 or that only stable MLH1 variants are able to bind PMS1 and PMS2, and

bioRxiv preprint doi: https://doi.org/10.1101/622266; this version posted April 29, 2019. The copyright holder for this preprint (which was not certified by peer review) is the author/funder, who has granted bioRxiv a license to display the preprint in perpetuity. It is made available under aCC-BY-NC-ND 4.0 International license.

that this binding in turn protects PMS1 and PMS2 from proteasomal degradation. To test these possibilities, we proceeded to assess the PMS2-binding activity of the selected MLH1 variants. To this end, HCT116 cells were co-transfected with both MLH1 and YFP-tagged PMS2. Importantly, the overexpressed YFP-PMS2 protein did not affect the MLH1 level and appeared stable in the absence of MLH1 (Fig. 4G), allowing us to directly compare the PMS2-binding activity of the selected MLH1 variants. To ensure that the cells contained sufficient levels of the unstable MLH1 variants, the cells were treated with bortezomib prior to lysis. We found that the wild-type and stable MLH1 variants (E23D, I219V) were efficiently co-precipitated with the YFP-tagged PMS2 (Fig. 4H). Several of the unstable MLH1 variants did not display appreciable affinity for PMS2, even after blocking their degradation, suggesting that these MLH1 variants are structurally perturbed or unfolded to an extent that disables complex formation with PMS2. Interestingly, the K618A variant displayed a strong interaction with PMS2 (Fig. 4H), indicating that this unstable variant retains the ability to bind PMS2, and therefore potentially engage in mismatch repair. We note that this result is supported by the K618A variant's ability to stabilize PMS2 (Fig. 4E) and the distal positioning of K618 to the PMS2 binding site (Gueneau et al., 2013).

HSP70 is required for degradation of destabilized MLH1 variants

Since structurally destabilized proteins are prone to expose hydrophobic regions that are normally buried in the native protein conformation, molecular chaperones, including the prominent HSP70 and HSP90 enzymes, often engage such proteins in an attempt to refold them or to target them for proteasomal degradation (Arndt et al., 2007). Indeed, both HSP70 and HSP90 are known to interact with many missense variants though with different specificities and cellular consequences (Karras et al., 2017), and a previous study has linked HSP90 to MLH1 function (Fedier et al., 2005).

bioRxiv preprint doi: https://doi.org/10.1101/622266; this version posted April 29, 2019. The copyright holder for this preprint (which was not certified by peer review) is the author/funder, who has granted bioRxiv a license to display the preprint in perpetuity. It is made available under aCC-BY-NC-ND 4.0 International license.

To test the involvement of molecular chaperones in degradation of the selected MLH1 variants, we analyzed their interaction with HSP70 and HSP90 by co-immunoprecipitation and Western blotting. Similar to above, the cells were treated with bortezomib to ensure detectable amounts of MLH1. Interestingly, four of the destabilized MLH1 variants (G67R, R100P, T117M and R265C) displayed a strong interaction with HSP70, up to approximately 7-fold greater compared to wild-type MLH1 (Fig. 5AB). Conversely, in the case of HSP90 we observed binding to all the tested MLH1 variants, including the wild-type (Fig. 5CD), indicating that HSP90 may be involved in the function or general *de novo* folding of wild-type MLH1, while HSP70 may be involved in regulation of certain destabilized MLH1 variants, potentially playing a role in their degradation.

To test this hypothesis, we measured the steady-state levels of the MLH1 variants following inhibition of HSP70 and HSP90, respectively. We treated cells with the HSP70 inhibitor YM01 or the HSP90 inhibitor geldanamycin (GA) and compared with the MLH1 levels in untreated cells. Interestingly, the levels of some destabilized MLH1 variants increased significantly following HSP70 inhibition. Especially three variants (G67R, R100P, T117M) were affected (Fig. 5E), all of which were also found to bind HSP70 (Fig. 5A) and had the lowest steady-state levels prior to HSP70 inhibition of the eight tested variants. Together, these results suggest that HSP70 actively partakes in detecting and directing certain destabilized MLH1 variants for degradation. However, we did not observe any effect of HSP90 inhibition on the MLH1 protein levels for any of the tested variants (Fig. 5F).

Structural stability calculations for predicting pathogenic mutations

Our results show that unstable protein variants are likely to be rapidly degraded, suggesting that predictions of changed thermodynamic stability of missense MLH1 variants could be used to estimate whether a particular MLH1 missense variant is pathogenic or not. In comparison with the sequence-based tools (e.g. PolyPhen2, PROVEAN) that are currently employed in the clinic (Adzhubei et al.,

bioRxiv preprint doi: https://doi.org/10.1101/622266; this version posted April 29, 2019. The copyright holder for this preprint (which was not certified by peer review) is the author/funder, who has granted bioRxiv a license to display the preprint in perpetuity. It is made available under aCC-BY-NC-ND 4.0 International license.

2010; Choi and Chan, 2015), the FoldX energy predictions provide an orthogonal structure-based and sequence-conservation-independent prediction of whether a mutation is likely to be pathogenic. Unlike most variant consequence predictors, FoldX was not trained on whether mutations were benign or pathogenic, but solely on biophysical stability measurements (Guerois et al., 2002). This considerably reduces the risk of overfitting to known pathogenic variants. More importantly, because of the mechanistic link to protein stability, FoldX predictions enable insights into why a particular mutation is problematic (Kiel et al., 2016; Kiel and Serrano, 2014; Nielsen et al., 2017; Pey et al., 2007; Stein et al., 2019).

As a first test for utilizing the biophysical calculations, we analyzed the predicted protein stabilities of MLH1 variants reported in the >140.000 exomes available in the Genome Aggregation Database (gnomAD) (Karczewski et al., 2019; Lek et al., 2016). Gratifyingly, this revealed that those variants reported to occur at a high frequency in the population all displayed low ΔΔG values (Fig. 6A), suggesting that these MLH1 proteins are stable. Accordingly, with only a few exceptions, the most common MLH1 alleles reported in gnomAD also appeared functional (high DME scores) (Fig. 6A). To further test the performance of the structural stability calculations for identifying pathogenic MLH1 variants, we then compared the ΔΔG values for ClinVar-annotated MLH1 variants. This revealed that the benign MLH1 variants all appeared structurally stable, while many pathogenic variants appeared destabilized (Fig. 6B).

While many pathogenic variants are severely destabilized, others are predicted to be as stable as non-pathogenic variants. This observation could be explained e.g. by inaccuracies of our stability calculations or by loss of function via other mechanisms such as direct loss of enzymatic activity, post-translational modifications or protein-protein interactions (Wagih et al., 2018). Thus, as a separate method for predicting the biological consequences of mutations, we explored if sequence analysis of the MLH1 protein family across evolution would reveal differences in selective pressure

bioRxiv preprint doi: https://doi.org/10.1101/622266; this version posted April 29, 2019. The copyright holder for this preprint (which was not certified by peer review) is the author/funder, who has granted bioRxiv a license to display the preprint in perpetuity. It is made available under aCC-BY-NC-ND 4.0 International license.

between benign and pathogenic variants. We performed an analysis of a multiple sequence alignment of MLH1 homologs, which considers both conservation at individual sites, but also non-trivial, co-evolution between pairs of residues (Balakrishnan et al., 2011; Stein et al., 2019). Turning this data into a statistical model allowed us to score all possible missense MLH1 variants. As this statistical sequence model is based on homologous sequences shaped by evolutionary pressures, it is expected to generally capture which residues, and pairs of residues, are tolerated (Balakrishnan et al., 2011). As opposed to stability calculations via e.g. FoldX, this approach is not directly linked to an underlying mechanistic model. Thus, we generally expect destabilizing residues to be recognized as detrimental by both FoldX and the evolutionary statistical energies, while variants in functionally active sites might only be recognized by the latter, if they do not affect protein stability (Stein et al., 2019). On the other hand, stability calculations could capture effects specific to human MLH1 that are more difficult to disentangle through the sequence analyses. In our implementation, low scores indicate mutations that during evolution appear tolerated, while high scores mark amino acid substitutions that are rare and therefore more likely to be detrimental to protein structure and/or function. Indeed, the average sequence-based score for the benign variants is lower (variations more likely to be tolerated) than the average for the ClinVar-curated pathogenic variants (Fig. 6C). The full matrix of evolutionary statistical energies is included in the supplemental material (supplemental material file 2).

Finally, to compare the capability of the above-described evolutionary statistical energies, FoldX, and the more traditional sequence-based methods (PolyPhen2 and PROVEAN) to separate pathogenic and non-pathogenic variants, we applied these approaches on a set of known benign and disease-causing MLH1 variants. We then used receiver-operating characteristic (ROC) analyses to compare how well the different methods are able to distinguish 16 benign variants from 66 known pathogenic variants (Fig. 6D). The results show that although all predictors perform fairly well, the structural

bioRxiv preprint doi: https://doi.org/10.1101/622266; this version posted April 29, 2019. The copyright holder for this preprint (which was not certified by peer review) is the author/funder, who has granted bioRxiv a license to display the preprint in perpetuity. It is made available under aCC-BY-NC-ND 4.0 International license.

calculations and evolutionary statistical energies are slightly better at distinguishing disease-linked missense variants from harmless variants. Lastly, we combined structure-based stability calculations and evolutionary statistical energies into a two-dimensional landscape of variant tolerance (Fig. 6E), which largely agrees with the classification by Takahashi *et al.* (Takahashi et al., 2007). There are three variants with low evolutionary statistical energies (typically indicating tolerance), but predicted and experimentally confirmed destabilization vs. wild-type MLH1 (T662P, I565F, G244V). Further, a number of stable variants have high DME scores (indicating wild-type-like function), but also high evolutionary statistical energies, indicating likely loss of function. However, as comparison to ClinVar showed that several of these are classified as pathogenic (supplemental material, Fig. S2). A possible explanation for this discrepancy is a difference in sensitivity between human variants and the employed yeast assays (Takahashi et al., 2007).

bioRxiv preprint doi: https://doi.org/10.1101/622266; this version posted April 29, 2019. The copyright holder for this preprint (which was not certified by peer review) is the author/funder, who has granted bioRxiv a license to display the preprint in perpetuity. It is made available under aCC-BY-NC-ND 4.0 International license.

Discussion

Missense variants in the *MLH1* gene are a leading cause of Lynch syndrome (LS) and colorectal cancer (Peltomaki, 2016). In recent years, germline mutations that cause structural destabilization and subsequent protein misfolding have surfaced as the cause of several diseases, including cystic fibrosis (Ahner et al., 2007), phenylketonuria (Pey et al., 2007; Scheller et al., 2019), early onset Parkinson's disease (Mathiassen et al., 2015; Olzmann et al., 2004) and MSH2-linked LS (Arlow et al., 2013; Nielsen et al., 2017). Although previous studies have shown some MLH1 variants to be destabilized (Perera and Bapat, 2008; Takahashi et al., 2007), this has not been systematically addressed and the contribution of MLH1 protein stability for LS remains to be resolved.

In this study, we performed *in silico* saturation mutagenesis and stability predictions of all single-site MLH1 missense variants in the structurally-resolved regions of MLH1. Comparisons with a selected group of naturally occurring MLH1 variants revealed that those variants that are predicted to be destabilized indeed display substantially reduced steady-state protein levels. The decreased cellular amounts are caused by rapid proteasomal degradation. In turn, the loss of MLH1 causes a dramatic destabilization and proteasomal degradation of both PMS1 and PMS2. This effect suggests that the MutLα and MutLβ heterodimers are likely to be rather stable protein complexes, as the PMS1 and PMS2 proteins would otherwise be required to be stable in the absence of MLH1. These observations are in line with several previous studies on individual MLH1 variants (Cravo et al., 2002; Kosinski et al., 2010; Perera and Bapat, 2008; Raevaara et al., 2005) including a thorough analysis by Takahashi *et al*. (Takahashi et al., 2007), and also agree with tissue staining of tumor cells from patients with germline *MLH1* mutations (de Jong et al., 2004; Hampel et al., 2008).

Our observations indicate that structural destabilization appears to be a common result of many disease-linked *MLH1* missense variants. Supported by earlier functional studies (Takahashi et al., 2007), we suggest that the loss-of-function phenotype in many cases can be explained by structural

bioRxiv preprint doi: https://doi.org/10.1101/622266; this version posted April 29, 2019. The copyright holder for this preprint (which was not certified by peer review) is the author/funder, who has granted bioRxiv a license to display the preprint in perpetuity. It is made available under aCC-BY-NC-ND 4.0 International license.

destabilization and subsequent degradation. Indeed, 20 out of the 31 variants with DME=0 or DME=1 have steady-state levels less than 70% of wildtype MLH1. Our data also include examples of loss-of-function variants with high steady-state levels, which is expected, as variants can affect function without modifying stability, e.g. by changing binding interfaces or active sites (Gueneau et al., 2013), and these would therefore be interesting to analyze biochemically in more detail. For example, M35R, N64S and F80V are all close to the ATP binding site in the N-terminal domain of MLH1 (supplemental material, Fig. S3), and might thus interfere with the catalytic activity. This would be consistent with a loss-of-function phenotype (Takahashi et al., 2007) but wild-type-like cellular protein levels (Table 1).

The correlation between the predicted structural stability with both cellular stability and protein function, suggests that the stability predictions may be used for classifying MLH1 missense variants. This is particularly relevant for LS, where according to the ClinVar database (Landrum et al., 2018) 711 out of 851 (~84%) reported MLH1 missense variants are assigned as so-called variants of uncertain significance (VUS) (Manolio et al., 2017). Of note, the fact that we did not observe the E23D VUS as destabilized does not preclude this variant from being pathogenic, since it may affect function without being structurally perturbed. Although the variant appears functional in yeast cells (Takahashi et al., 2007), the evolutionary statistical energy of 0.9 indicates that this change is rare across the MLH1 protein family evolution and thus might be detrimental. Our results for the K618A VUS suggest that this variant, albeit being unstable, is still able to associate with PMS2 and may therefore be functional, but untimely degraded. Of the 69 MLH1 variants that we analyzed, 30 have status as VUSs. Of these, our analysis identified several (e.g. G54E, G244V, and L676R) that hold characteristics indicating that they are pathogenic: steady-state levels below 50% of WT, high $\Delta\Delta G$ and low functionality score *in vivo* (Takahashi et al., 2007) (Table 1).

bioRxiv preprint doi: https://doi.org/10.1101/622266; this version posted April 29, 2019. The copyright holder for this preprint (which was not certified by peer review) is the author/funder, who has granted bioRxiv a license to display the preprint in perpetuity. It is made available under aCC-BY-NC-ND 4.0 International license.

The potential use of stability predictions for LS diagnostics is supported by the predicted MLH1 stabilities clearly separating into disease-linked and benign MLH1 variants. Moreover, since we observe that those MLH1 alleles that occur more frequently in the population are in general predicted as stable, this suggests that these common MLH1 alleles are either benign or at least only disease causing with a low penetrance. However, certainly not all the unstable variants were accurately detected by the structural predictions. For instance, out of our eight selected variants, three (R100P, R265C, K618A) appeared unstable, but were not predicted to be so (Table 1). Here, it is important to note that the stability predictions report on the global stability of the protein, while in a cellular context it is unlikely that any of the variants are fully unfolded. Instead, it is likely that local elements unfold (Stein et al., 2019), and although refolding may occur, the locally unfolded state allows chaperones and other protein quality control components to associate and target the protein for proteasomal degradation (Fig. 7). A better understanding of the importance of local unfolding events for cellular stability is an important area for further research.

Similar to other destabilized proteins, we found that the degradation of some structurally destabilized MLH1 variants depends on the molecular chaperone HSP70. This suggests that HSP70 recognizes the destabilized MLH1 variants and targets them for proteasomal degradation. Accordingly, we observed that several destabilized MLH1 variants associate with HSP70. Involvement of molecular chaperones in protein degradation is a well-established phenomenon (Arndt et al., 2007; Kandasamy and Andreasson, 2018; Samant et al., 2018). Moreover, our findings are consistent with recent developments in the field, showing that degradation signals, so-called degrons, are buried within the native structure of most globular proteins. Upon exposure when the protein structure is destabilized, the degrons are recognized by chaperones and other protein quality control components, which in turn guide the target protein for degradation (Enam et al., 2018; Geffen et al., 2016; Kim et al., 2013; Maurer et al., 2016; Ravid and Hochstrasser, 2008). Thus, ultimately the degradation of a protein will

bioRxiv preprint doi: https://doi.org/10.1101/622266; this version posted April 29, 2019. The copyright holder for this preprint (which was not certified by peer review) is the author/funder, who has granted bioRxiv a license to display the preprint in perpetuity. It is made available under aCC-BY-NC-ND 4.0 International license.

depend on both the structural destabilization (ΔΔG) as well as the exposed degrons, and how efficiently these are recognized by the degradation machinery. The results presented here suggest that biophysical calculations are able to predict the structural destabilization (ΔΔG), however, since the nature of protein quality control degrons is still largely undefined (Geffen et al., 2016; Maurer et al., 2016; Rosenbaum et al., 2011; van der Lee et al., 2014), *in silico* prediction of these is currently not possible.

In conclusion, our results support a model (Fig. 7) where missense mutations can cause destabilization of the MLH1 protein, leading to exposure of degrons which, in turn, trigger HSP70-assisted proteasomal degradation, causing disruption of the MMR pathway and ultimately leading to an increased cumulative lifetime risk of cancer development in LS patients.

bioRxiv preprint doi: https://doi.org/10.1101/622266; this version posted April 29, 2019. The copyright holder for this preprint (which was not certified by peer review) is the author/funder, who has granted bioRxiv a license to display the preprint in perpetuity. It is made available under aCC-BY-NC-ND 4.0 International license.

Materials and Methods

Plasmids

Plasmids for expression of wild-type and mutant MLH1 variants have been described before (Takahashi et al., 2007). pCMV-MYC-DDK-HSP70 and pcDNA3-HA-HSP90 were kindly provided by Dr. Kenneth Thirstrup (H. Lundbeck A/S). The pEYFP-C2-PMS2 plasmid was kindly provided by Prof. Lene J. Rasmussen (University of Copenhagen). pEGFP was purchased from Clontech. A pcDNA3-V5 vector served as a negative control.

Cell culture

HCT116 cells (kindly provided by Prof. Mads Gyrd-Hansen (University of Oxford)) were maintained in McCoy's 5A medium (Gibco) supplemented with 10% fetal calf serum (Invitrogen), 2 mM glutamine, 5000 IU/ml penicillin and 5 mg/ml streptomycin at 37 °C in a humidified atmosphere with 5% CO_2. Transfections were performed using FugeneHD (Promega) as described by the manufacturer in reduced serum medium OptiMEM (Gibco). Cells were harvested no later than 72 hours after transfection at a final confluence around 90%.

About 24 hours after transfection, cells were treated with serum-free growth medium containing 25 µg/mL cycloheximide (Sigma) for a duration of 4, 8 or 12 hours, 10 µM bortezomib (LC laboratories) for 8 or 16 hours, 5 µM YM01 (StressMarq) for 24 hours or 1 µM geldanamycin (Sigma) for 24 hours. Cells were lysed in SDS sample buffer (94 mM Tris/HCl pH 6.8, 3% SDS, 19% glycerol and 0.75% β-mercaptoethanol) and protein levels were analyzed by SDS-PAGE and Western blotting.

SDS-PAGE and Western blotting

bioRxiv preprint doi: https://doi.org/10.1101/622266; this version posted April 29, 2019. The copyright holder for this preprint (which was not certified by peer review) is the author/funder, who has granted bioRxiv a license to display the preprint in perpetuity. It is made available under aCC-BY-NC-ND 4.0 International license.

Proteins were resolved by SDS-PAGE on 7x8 cm 12.5% acrylamide gels, and transferred to 0.2 µm nitrocellulose membranes (Advantec, Toyo Roshi Kaisha Ltd.). Blocking was performed using PBS (8 g/L NaCl, 0.2 g/L KCl, 1.44 g/L Na_2HPO_4, 0.24 g/L KH_2PO_4, pH 7.4) with 5% dry milk powder and 0.05% Tween-20. Membranes were probed with primary antibodies against MLH1 (Santa Cruz Biotechnology, Product no.: sc-11442), β-actin (Sigma Aldrich, Product no.: A5441), PMS2 (BD Biosciences, Product no.: 556415), PMS1 (Invitrogen, Product no.: PA5-35952), GFP (Chromotek, Product no.: 3H9), Myc (Chromotek, Product no.: 9E1) or HA (Roche Diagnostics, Product no.: 3F10) at 4 °C overnight. HRP-conjugated secondary antibodies were purchased from DAKO. ECL detection reagent (GE Life Sciences) was used for development.

Immunofluorescence and imaging

Transfected cells were seeded 24 hours prior to fixing with 4 % formaldehyde in PBS in thin-bottomed 384-well plates. The fixed cells were then washed three times in PBS and permeabilized with 0.25 % Triton-X-100 in PBS for 5 minutes at room temperature (RT). After washing with PBS, 5 % bovine serum albumin (BSA, Sigma) in PBS was used for 45 minutes at RT for blocking. The cells were then washed with PBS and incubated with a 1:100 dilution of the anti-MLH1 antibody (Santa Cruz Biotechnology, Product no.: sc-11442) in 1 % BSA in PBS for 1 hour at RT. The cells were washed with PBS and incubated with a 1:1000 dilution Alexa Fluor 568 anti-rabbit antibody (Invitrogen) in 1 % BSA in PBS for 1 hour at RT. After additional washing with PBS, the DNA was stained with Höchst 33342 (Sigma) for 10 minutes. Microscopy was performed using an InCell2200 microscope (GE Healthcare). The filters were Höchst (ex 390 nm, em 432 nm) and TexasRed (ex 575 nm, em 620 nm). The InCell Developer Toolbox (GE Healthcare) was used for image analysis. To determine the abundance of the MLH1 variants, the total intensity of the red channel in each cell was measured after excluding the non-transfected cells.

bioRxiv preprint doi: https://doi.org/10.1101/622266; this version posted April 29, 2019. The copyright holder for this preprint (which was not certified by peer review) is the author/funder, who has granted bioRxiv a license to display the preprint in perpetuity. It is made available under aCC-BY-NC-ND 4.0 International license.

Co-immunoprecipitation

Transfected cells were lysed in buffer A (50 mM Tris/HCl pH 7.5, 150 mM NaCl, 1 mM EDTA and 0.5% NP-40 supplemented with Complete Mini EDTA-free Protease inhibitor cocktail tablets (Roche)) and left to incubate for 20 minutes on ice. The lysates were cleared by centrifugation (13000 g, 30 min) and the proteins were captured with GFP-trap (Chromotek), Myc-trap (Chromotek) or HA-agarose beads (Sigma) by tumbling end-over-end overnight at 4℃. The beads were washed three times by centrifugation (1000 g, 10 sec) in buffer A. Finally, the beads were resuspended in SDS sample buffer (94 mM Tris/HCl pH 6.8, 3% SDS, 19% glycerol and 0.75% β-mercaptoethanol) and analyzed by SDS-PAGE and Western blotting.

Stability calculations

The changes in folding stability (ΔΔG) were calculated using FoldX (Guerois et al., 2002) based on PDB IDs 4P7A (Wu et al., 2015) for the N-terminal domain of MLH1, and 3RBN for the C-terminal domain. The ΔΔGs were calculated from each structure individually by first applying the RepairPDB function to fix minor issues in the original coordinates, and then the BuildModel function to generate each individual amino acid variant. Each calculation was repeated 5 times, and the average difference in stability between wild type and variant is reported, such that values <0 kcal/mol indicate stabilized variants, and values >0 kcal/mol indicate destabilized variants with respect to the wild type MLH1 protein. Values > 15 kcal/mol likely indicate clashes in the model FoldX generated. While this does indicate that major destabilization is likely, the actual values are less meaningful for these clashing variants, and we thus truncated them to 15 kcal/mol in our figures. Positions where most predicted effects are stabilizing indicate that the FoldX energy function disagrees with the residue in the crystal

bioRxiv preprint doi: https://doi.org/10.1101/622266; this version posted April 29, 2019. The copyright holder for this preprint (which was not certified by peer review) is the author/funder, who has granted bioRxiv a license to display the preprint in perpetuity. It is made available under aCC-BY-NC-ND 4.0 International license.

structure. We therefore exclude such positions from the ΔΔG analysis (marked NA in supplemental material file 1).

Evolutionary statistical energy calculations

To assess the likelihood of finding any given variant in the protein family, we created a multiple sequence alignment of human MLH1 using HHblits (Zimmermann et al., 2018) and then calculated a sequence log-likelihood score combining site-conservation and pairwise co-variation using Gremlin (Balakrishnan et al., 2011). Scores were normalized to a range of (0,1), with low scores indicating tolerated sequences and high scores indicating variants that are rare or unobserved across the multiple sequence alignment. Positions at which the number of distinct homologous sequences was too small to extract meaningful evolutionary statistical energies are set to NA (supplemental material file 2). Other sequence-based predictions of functional variant consequences were retrieved from the webservers of PROVEAN (Choi and Chan, 2015) and PolyPhen2 (Adzhubei et al., 2010).

Dominant mutator effect (DME)

We grouped the functional classification observations from Takahashi *et al.* (Takahashi et al., 2007) into 4 categories by summarizing the number of assays each variant showed functional behavior in. Thus, variants in group 0 were non-functional in all three assays, those in group 3 were functional in all three assays, and the rest were functional in some, but not in other assays.

bioRxiv preprint doi: https://doi.org/10.1101/622266; this version posted April 29, 2019. The copyright holder for this preprint (which was not certified by peer review) is the author/funder, who has granted bioRxiv a license to display the preprint in perpetuity. It is made available under aCC-BY-NC-ND 4.0 International license.

Acknowledgements

The authors thank Prof. Lene J. Rasmussen, Prof. Mads Gyrd-Hansen, and Dr. Kenneth Thirstrup for sharing cells and reagents, and Dr. Elin J. Pietras, Dr. Cornelia Steinhauer, Cecilie Søltoft, and Anne-Marie Lauridsen for excellent technical assistance.

Competing interests

No competing interests declared.

Author contributions

A.B.A., A.S., K.S.K., S.V.N.. A.Sh. and E.P. conducted the experiments. A.B.A., A.S., S.V.N., M.T., C.I., K.L.-L. and R.H.-P. analyzed the data. A.B.A., A.S., K.L.-L. and R.H.-P. designed the experiments. E.R.H., I.B., A.G., K.L.-L. and R.H.-P. conceived the study. M.T. and C.I. contributed reagents. A.B.A, A.S., K.L.-L. and R.H.-P. wrote the paper.

Funding

This work was supported by grants from the Novo Nordisk Foundation Challenge Program PRISM (to A.S., K.L.-L., and R.H.-P.), the Lundbeck Foundation (to A.S., K.L.-L., and R.H.-P.), the Danish Cancer Society (to R.H.-P.), the A.P. Møller Foundation (to R.H.-P.), Novo Nordisk Foundation Young Investigator Award (NNF15OC0016662; to E.R.H.) and the Danish Council for Independent Research (to R.H.-P).

bioRxiv preprint doi: https://doi.org/10.1101/622266; this version posted April 29, 2019. The copyright holder for this preprint (which was not certified by peer review) is the author/funder, who has granted bioRxiv a license to display the preprint in perpetuity. It is made available under aCC-BY-NC-ND 4.0 International license.

Table 1

Characteristics of the selected naturally occurring MLH1 variants

Variant*	Steady-state level (% of WT)	FoldX ΔΔG (kcal/mol)	ClinVar annotation¤	DME#
E23D	**90.0**	**0.49**	**VUS**	**3**
I25T	51.3	2.40	VUS	3
A29S	109.6	2.06	(likely) pathogenic	3
M35R	72.1	3.52	(likely) pathogenic	0
I36S	63.2	4.08	VUS	NA
N38D	63.5	1.61	VUS	2
S44F	9.8	>15	(likely) pathogenic	0
S44A	103.2	-1.35	VUS	3
G54E	15.3	>15	VUS	1
N64S	96.3	2.16	VUS	1
G67R	**35.0**	**>15**	**(likely) pathogenic**	**0**
G67W	14.5	>15	(likely) pathogenic	0
I68N	62.5	2.22	(likely) pathogenic	0
R69K	104.9	-0.18	VUS	3
C77Y	61.0	6.57	(likely) pathogenic	2
F80V	72.3	2.22	(likely) pathogenic	1
T82I	100.0	0.54	(likely) pathogenic	2
R100P	**46.4**	**-1.25**	**(likely) pathogenic**	**2**
E102D	97.9	0.34	(likely) pathogenic	3
A111V	68.8	4.96	(likely) pathogenic	0
T117M	**32.8**	**7.14**	**(likely) pathogenic**	**0**
T117R	46.2	12.70	(likely) pathogenic	0
A128P	62.8	2.40	(likely) pathogenic	0
D132H	110.2	-0.30	(likely) benign	3
A160V	107.3	NA	VUS	3
R182G	87.9	2.60	(likely) pathogenic	3
S193P	100.7	2.73	VUS	0
V213M	103.9	-0.81	(likely) benign	3
R217C	74.1	1.06	VUS	2
I219V	**112.5**	**0.66**	**(likely) benign**	**3**
I219L	121.9	-0.05	(likely) benign	3
R226L	63.3	0.27	(likely) pathogenic	1
G244V	32.0	>15	VUS	0
G244D	38.8	>15	(likely) pathogenic	0
H264R	117.6	-0.60	VUS	3
R265C	**57.2**	**0.28**	**(likely) pathogenic**	**2**
R265H	81.4	0.04	VUS	3
E268G	81.1	0.81	(likely) benign	2
L272V	80.0	1.95	VUS	3
A281V	82.5	0.87	(likely) pathogenic	3
K286Q	101.8	0.28	VUS	2
S295G	88.6	0.13	(likely) pathogenic	2
H329P	54.1	5.67	(likely) pathogenic	1
V506A	62.1	2.18	VUS	2
Q542L	110.2	-1.56	VUS	3
L549P	63.7	5.17	VUS	0
I565F	65.9	9.64	VUS	0
L574P	34.4	11.97	(likely) pathogenic	0
E578G	103.2	0.45	(likely) benign	2
L582V	100.0	1.93	VUS	3
L588P	88.6	3.30	VUS	1
K618A	**80.4**	**0.61**	**VUS**	**1**
K618T	106.5	0.09	(likely) benign	0
L622H	61.1	4.97	(likely) pathogenic	0
P640T	61.1	3.78	VUS	0

bioRxiv preprint doi: https://doi.org/10.1101/622266; this version posted April 29, 2019. The copyright holder for this preprint (which was not certified by peer review) is the author/funder, who has granted bioRxiv a license to display the preprint in perpetuity. It is made available under aCC-BY-NC-ND 4.0 International license.

L653R	66.1	3.22	(likely) pathogenic	0
I655V	89.1	1.03	(likely) benign	3
I655T	71.1	1.29	VUS	3
R659P	**69.0**	**6.93**	**(likely) pathogenic**	**0**
R659Q	84.9	2.41	VUS	2
T662P	72.7	5.23	(likely) pathogenic	0
E663G	72.0	NA¶	VUS	3
E663D	97.2	NA¶	(likely) pathogenic	2
L676R	36.8	5.12	VUS	0
R687W	115.4	1.12	(likely) pathogenic	0
Q689R	71.0	NA¶	(likely) benign	3
V716M	100.1	1.41	(likely) benign	1
H718Y	73.7	0.16	(likely) benign	2
K751R	82.1	-0.23	(likely) benign	3

*: boldfaced variants studied in detail; ¤: VUS: variant of unknown significance; #DME: dominant mutator effect; ¶: position excluded (see materials and methods).

bioRxiv preprint doi: https://doi.org/10.1101/622266; this version posted April 29, 2019. The copyright holder for this preprint (which was not certified by peer review) is the author/funder, who has granted bioRxiv a license to display the preprint in perpetuity. It is made available under aCC-BY-NC-ND 4.0 International license.

References

1. Aarnio, M., Sankila, R., Pukkala, E., Salovaara, R., Aaltonen, L.A., de la Chapelle, A., Peltomaki, P., Mecklin, J.P., and Jarvinen, H.J. (1999). Cancer risk in mutation carriers of DNA-mismatch-repair genes. Int. J. Cancer 81, 214-218.

2. Adzhubei, I.A., Schmidt, S., Peshkin, L., Ramensky, V.E., Gerasimova, A., Bork, P., Kondrashov, A.S., and Sunyaev, S.R. (2010). A method and server for predicting damaging missense mutations. Nat. Methods 7, 248-249.

3. Ahner, A., Nakatsukasa, K., Zhang, H., Frizzell, R.A., and Brodsky, J.L. (2007). Small heat-shock proteins select deltaF508-CFTR for endoplasmic reticulum-associated degradation. Mol. Biol. Cell 18, 806-814.

4. Allen, M., Poggiali, D., Whitaker, K., Marshall, T.R., and Kievit, R. (2018). Raincloud plots: a multi-platform tool for robust data visualization. PeerJ Preprints 6, e27137v1.

5. Arlow, T., Scott, K., Wagenseller, A., and Gammie, A. (2013). Proteasome inhibition rescues clinically significant unstable variants of the mismatch repair protein Msh2. Proc. Natl. Acad. Sci. U. S. A 110, 246-251.

6. Arndt, V., Rogon, C., and Hohfeld, J. (2007). To be, or not to be--molecular chaperones in protein degradation. Cell Mol. Life Sci. 64, 2525-2541.

7. Balakrishnan, S., Kamisetty, H., Carbonell, J.G., Lee, S.I., and Langmead, C.J. (2011). Learning generative models for protein fold families. Proteins 79, 1061-1078.

8. Barrow, E., Alduaij, W., Robinson, L., Shenton, A., Clancy, T., Lalloo, F., Hill, J., and Evans, D.G. (2008). Colorectal cancer in HNPCC: cumulative lifetime incidence, survival and tumour distribution. A report of 121 families with proven mutations. Clin. Genet. 74, 233-242.

9. Bullock, A.N., Henckel, J., and Fersht, A.R. (2000). Quantitative analysis of residual folding and DNA binding in mutant p53 core domain: definition of mutant states for rescue in cancer therapy. Oncogene 19, 1245-1256.

10. Cannavo, E., Gerrits, B., Marra, G., Schlapbach, R., and Jiricny, J. (2007). Characterization of the interactome of the human MutL homologues MLH1, PMS1, and PMS2. J. Biol. Chem. 282, 2976-2986.

11. Casadio, R., Vassura, M., Tiwari, S., Fariselli, P., and Luigi, M.P. (2011). Correlating disease-related mutations to their effect on protein stability: a large-scale analysis of the human proteome. Hum. Mutat. 32, 1161-1170.

12. Choi, Y., and Chan, A.P. (2015). PROVEAN web server: a tool to predict the functional effect of amino acid substitutions and indels. Bioinformatics. 31, 2745-2747.

13. Cravo, M., Afonso, A.J., Lage, P., Albuquerque, C., Maia, L., Lacerda, C., Fidalgo, P., Chaves, P., Cruz, C., and Nobre-Leitao, C. (2002). Pathogenicity of missense and splice site mutations in hMSH2 and hMLH1 mismatch repair genes: implications for genetic testing. Gut 50, 405-412.

14. de Jong, A.E., van, P.M., Hendriks, Y., Tops, C., Wijnen, J., Ausems, M.G., Meijers-Heijboer, H., Wagner, A., van Os, T.A., Brocker-Vriends, A.H., Vasen, H.F., and Morreau, H. (2004).

bioRxiv preprint doi: https://doi.org/10.1101/622266; this version posted April 29, 2019. The copyright holder for this preprint (which was not certified by peer review) is the author/funder, who has granted bioRxiv a license to display the preprint in perpetuity. It is made available under aCC-BY-NC-ND 4.0 International license.

Microsatellite instability, immunohistochemistry, and additional PMS2 staining in suspected hereditary nonpolyposis colorectal cancer. Clin. Cancer Res. 10, 972-980.

15. Dowty, J.G., Win, A.K., Buchanan, D.D., Lindor, N.M., Macrae, F.A., Clendenning, M., Antill, Y.C., Thibodeau, S.N., Casey, G., Gallinger, S., Marchand, L.L., Newcomb, P.A., Haile, R.W., Young, G.P., James, P.A., Giles, G.G., Gunawardena, S.R., Leggett, B.A., Gattas, M., Boussioutas, A., Ahnen, D.J., Baron, J.A., Parry, S., Goldblatt, J., Young, J.P., Hopper, J.L., and Jenkins, M.A. (2013). Cancer risks for MLH1 and MSH2 mutation carriers. Hum. Mutat. 34, 490-497.

16. Dunlop, M.G., Farrington, S.M., Carothers, A.D., Wyllie, A.H., Sharp, L., Burn, J., Liu, B., Kinzler, K.W., and Vogelstein, B. (1997). Cancer risk associated with germline DNA mismatch repair gene mutations. Hum. Mol. Genet. 6, 105-110.

17. Enam, C., Geffen, Y., Ravid, T., and Gardner, R.G. (2018). Protein Quality Control Degradation in the Nucleus. Annu. Rev. Biochem. 87, 725-749.

18. Fedier, A., Stuedli, A., and Fink, D. (2005). Presence of MLH1 protein aggravates the potential of the HSP90 inhibitor radicicol to sensitize tumor cells to cisplatin. Int. J. Oncol. 27, 1697-1705.

19. Geffen, Y., Appleboim, A., Gardner, R.G., Friedman, N., Sadeh, R., and Ravid, T. (2016). Mapping the Landscape of a Eukaryotic Degronome. Mol. Cell 63, 1055-1065.

20. Gueneau, E., Dherin, C., Legrand, P., Tellier-Lebegue, C., Gilquin, B., Bonnesoeur, P., Londino, F., Quemener, C., Le Du, M.H., Marquez, J.A., Moutiez, M., Gondry, M., Boiteux, S., and Charbonnier, J.B. (2013). Structure of the MutLalpha C-terminal domain reveals how Mlh1 contributes to Pms1 endonuclease site. Nat. Struct. Mol. Biol. 20, 461-468.

21. Guerois, R., Nielsen, J.E., and Serrano, L. (2002). Predicting changes in the stability of proteins and protein complexes: a study of more than 1000 mutations. J. Mol. Biol. 320, 369-387.

22. Hampel, H., Frankel, W.L., Martin, E., Arnold, M., Khanduja, K., Kuebler, P., Clendenning, M., Sotamaa, K., Prior, T., Westman, J.A., Panescu, J., Fix, D., Lockman, J., LaJeunesse, J., Comeras, I., and de la Chapelle, A. (2008). Feasibility of screening for Lynch syndrome among patients with colorectal cancer. J. Clin. Oncol. 26, 5783-5788.

23. Heinen, C.D. (2010). Genotype to phenotype: analyzing the effects of inherited mutations in colorectal cancer families. Mutat. Res. 693, 32-45.

24. Hinrichsen, I., Wessbecher, I.M., Huhn, M., Passmann, S., Zeuzem, S., Plotz, G., Biondi, R.M., and Brieger, A. (2017). Phosphorylation-dependent signaling controls degradation of DNA mismatch repair protein PMS2. Mol. Carcinog. 56, 2663-2668.

25. Jiricny, J. (2006). The multifaceted mismatch-repair system. Nat. Rev. Mol. Cell Biol. 7, 335-346.

26. Jiricny, J. (2013). Postreplicative mismatch repair. Cold Spring Harb. Perspect. Biol. 5, a012633.

27. Jun, S.H., Kim, T.G., and Ban, C. (2006). DNA mismatch repair system. Classical and fresh roles. FEBS J. 273, 1609-1619.

28. Kampmeyer, C., Nielsen, S.V., Clausen, L., Stein, A., Gerdes, A.M., Lindorff-Larsen, K., and Hartmann-Petersen, R. (2017). Blocking protein quality control to counter hereditary cancers. Genes Chromosomes. Cancer 56, 823-831.

bioRxiv preprint doi: https://doi.org/10.1101/622266; this version posted April 29, 2019. The copyright holder for this preprint (which was not certified by peer review) is the author/funder, who has granted bioRxiv a license to display the preprint in perpetuity. It is made available under aCC-BY-NC-ND 4.0 International license.

29. Kandasamy, G., and Andreasson, C. (2018). Hsp70-Hsp110 chaperones deliver ubiquitin-dependent and -independent substrates to the 26S proteasome for proteolysis in yeast. J. Cell Sci. 131.

30. Karczewski, K.J., Francioli, L.C., Tiao, G., Cummings, B.B., Alfoldi, J., Wang, Q., Collins, R.L., Laricchia, K.M., Ganna, A., Birnbaum, D.P., Gauthier, L.D., Brand, H., Solomonson, M., Watts, N.A., Rhodes, D., Singer-Berk, M., Seaby, E.G., Kosmicki, J.A., Walters, R.K., Tashman, K., Farjoun, Y., Banks, E., Poterba, T., Wang, A., Seed, C., Whiffin, N., Chong, J.X., Samocha, K.E., Pierce-Hoffman, E., Zappala, Z., Donnell-Luria, A.H., Minikel, E.V., Weisburd, B., Lek, M., Ware, J.S., Vittal, C., Armean, I.M., Bergelson, L., Cibulskis, K., Connolly, K.M., Covarrubias, M., Donnelly, S., Ferriera, S., Gabriel, S., Gentry, J., Gupta, N., Jeandet, T., Kaplan, D., Llanwarne, C., Munshi, R., Novod, S., Petrillo, N., Roazen, D., Ruano-Rubio, V., Saltzman, A., Schleicher, M., Soto, J., Tibbetts, K., Tolonen, C., Wade, G., Talkowski, M.E., The Genome Database Consortium, Neale, B.M., Daly, M.J., and MacArthur, D.G. (2019). Variation across 141,456 human exomes and genomes reveals the spectrum of loss-of-function intolerance across human protein-coding genes. bioRxiv 531210.

31. Karras, G.I., Yi, S., Sahni, N., Fischer, M., Xie, J., Vidal, M., D'Andrea, A.D., Whitesell, L., and Lindquist, S. (2017). HSP90 Shapes the Consequences of Human Genetic Variation. Cell 168, 856-866.

32. Kiel, C., Benisty, H., Llorens-Rico, V., and Serrano, L. (2016). The yin-yang of kinase activation and unfolding explains the peculiarity of Val600 in the activation segment of BRAF. Elife. 5, e12814.

33. Kiel, C., and Serrano, L. (2014). Structure-energy-based predictions and network modelling of RASopathy and cancer missense mutations. Mol. Syst. Biol. 10, 727.

34. Kim, I., Miller, C.R., Young, D.L., and Fields, S. (2013). High-throughput analysis of in vivo protein stability. Mol. Cell Proteomics. 12, 3370-3378.

35. Kondo, E., Horii, A., and Fukushige, S. (2001). The interacting domains of three MutL heterodimers in man: hMLH1 interacts with 36 homologous amino acid residues within hMLH3, hPMS1 and hPMS2. Nucleic Acids Res. 29, 1695-1702.

36. Kosinski, J., Hinrichsen, I., Bujnicki, J.M., Friedhoff, P., and Plotz, G. (2010). Identification of Lynch syndrome mutations in the MLH1-PMS2 interface that disturb dimerization and mismatch repair. Hum. Mutat. 31, 975-982.

37. Kriegenburg, F., Jakopec, V., Poulsen, E.G., Nielsen, S.V., Roguev, A., Krogan, N., Gordon, C., Fleig, U., and Hartmann-Petersen, R. (2014). A chaperone-assisted degradation pathway targets kinetochore proteins to ensure genome stability. PLoS. Genet. 10, e1004140.

38. Landrum, M.J., Lee, J.M., Benson, M., Brown, G.R., Chao, C., Chitipiralla, S., Gu, B., Hart, J., Hoffman, D., Jang, W., Karapetyan, K., Katz, K., Liu, C., Maddipatla, Z., Malheiro, A., McDaniel, K., Ovetsky, M., Riley, G., Zhou, G., Holmes, J.B., Kattman, B.L., and Maglott, D.R. (2018). ClinVar: improving access to variant interpretations and supporting evidence. Nucleic Acids Res. 46, D1062-D1067.

39. Lek, M., Karczewski, K.J., Minikel, E.V., Samocha, K.E., Banks, E., Fennell, T., O'Donnell-Luria, A.H., Ware, J.S., Hill, A.J., Cummings, B.B., Tukiainen, T., Birnbaum, D.P., Kosmicki, J.A., Duncan, L.E., Estrada, K., Zhao, F., Zou, J., Pierce-Hoffman, E., Berghout, J., Cooper, D.N., Deflaux, N., DePristo, M., Do, R., Flannick, J., Fromer, M., Gauthier, L., Goldstein, J., Gupta, N., Howrigan, D., Kiezun, A., Kurki, M.I., Moonshine, A.L., Natarajan, P., Orozco, L.,

bioRxiv preprint doi: https://doi.org/10.1101/622266; this version posted April 29, 2019. The copyright holder for this preprint (which was not certified by peer review) is the author/funder, who has granted bioRxiv a license to display the preprint in perpetuity. It is made available under aCC-BY-NC-ND 4.0 International license.

Peloso, G.M., Poplin, R., Rivas, M.A., Ruano-Rubio, V., Rose, S.A., Ruderfer, D.M., Shakir, K., Stenson, P.D., Stevens, C., Thomas, B.P., Tiao, G., Tusie-Luna, M.T., Weisburd, B., Won, H.H., Yu, D., Altshuler, D.M., Ardissino, D., Boehnke, M., Danesh, J., Donnelly, S., Elosua, R., Florez, J.C., Gabriel, S.B., Getz, G., Glatt, S.J., Hultman, C.M., Kathiresan, S., Laakso, M., McCarroll, S., McCarthy, M.I., McGovern, D., McPherson, R., Neale, B.M., Palotie, A., Purcell, S.M., Saleheen, D., Scharf, J.M., Sklar, P., Sullivan, P.F., Tuomilehto, J., Tsuang, M.T., Watkins, H.C., Wilson, J.G., Daly, M.J., and MacArthur, D.G. (2016). Analysis of protein-coding genetic variation in 60,706 humans. Nature 536, 285-291.

40. Li, G.M., and Modrich, P. (1995). Restoration of mismatch repair to nuclear extracts of H6 colorectal tumor cells by a heterodimer of human MutL homologs. Proc. Natl. Acad. Sci. U. S. A 92, 1950-1954.

41. Lynch, H.T., Snyder, C.L., Shaw, T.G., Heinen, C.D., and Hitchins, M.P. (2015). Milestones of Lynch syndrome: 1895-2015. Nat. Rev. Cancer 15, 181-194.

42. Manolio, T.A., Fowler, D.M., Starita, L.M., Haendel, M.A., MacArthur, D.G., Biesecker, L.G., Worthey, E., Chisholm, R.L., Green, E.D., Jacob, H.J., McLeod, H.L., Roden, D., Rodriguez, L.L., Williams, M.S., Cooper, G.M., Cox, N.J., Herman, G.E., Kingsmore, S., Lo, C., Lutz, C., MacRae, C.A., Nussbaum, R.L., Ordovas, J.M., Ramos, E.M., Robinson, P.N., Rubinstein, W.S., Seidman, C., Stranger, B.E., Wang, H., Westerfield, M., and Bult, C. (2017). Bedside Back to Bench: Building Bridges between Basic and Clinical Genomic Research. Cell 169, 6-12.

43. Mathiassen, S.G., Larsen, I.B., Poulsen, E.G., Madsen, C.T., Papaleo, E., Lindorff-Larsen, K., Kragelund, B.B., Nielsen, M.L., Kriegenburg, F., and Hartmann-Petersen, R. (2015). A Two-step Protein Quality Control Pathway for a Misfolded DJ-1 Variant in Fission Yeast. J. Biol. Chem. 290, 21141-21153.

44. Matreyek, K.A., Starita, L.M., Stephany, J.J., Martin, B., Chiasson, M.A., Gray, V.E., Kircher, M., Khechaduri, A., Dines, J.N., Hause, R.J., Bhatia, S., Evans, W.E., Relling, M.V., Yang, W., Shendure, J., and Fowler, D.M. (2018). Multiplex assessment of protein variant abundance by massively parallel sequencing. Nat. Genet. 50, 874-882.

45. Maurer, M.J., Spear, E.D., Yu, A.T., Lee, E.J., Shahzad, S., and Michaelis, S. (2016). Degradation Signals for Ubiquitin-Proteasome Dependent Cytosolic Protein Quality Control (CytoQC) in Yeast. G3. (Bethesda.).

46. McShane, E., Sin, C., Zauber, H., Wells, J.N., Donnelly, N., Wang, X., Hou, J., Chen, W., Storchova, Z., Marsh, J.A., Valleriani, A., and Selbach, M. (2016). Kinetic Analysis of Protein Stability Reveals Age-Dependent Degradation. Cell 167, 803-815.

47. Mitchell, A.L., Attwood, T.K., Babbitt, P.C., Blum, M., Bork, P., Bridge, A., Brown, S.D., Chang, H.Y., El-Gebali, S., Fraser, M.I., Gough, J., Haft, D.R., Huang, H., Letunic, I., Lopez, R., Luciani, A., Madeira, F., Marchler-Bauer, A., Mi, H., Natale, D.A., Necci, M., Nuka, G., Orengo, C., Pandurangan, A.P., Paysan-Lafosse, T., Pesseat, S., Potter, S.C., Qureshi, M.A., Rawlings, N.D., Redaschi, N., Richardson, L.J., Rivoire, C., Salazar, G.A., Sangrador-Vegas, A., Sigrist, C.J.A., Sillitoe, I., Sutton, G.G., Thanki, N., Thomas, P.D., Tosatto, S.C.E., Yong, S.Y., and Finn, R.D. (2019). InterPro in 2019: improving coverage, classification and access to protein sequence annotations. Nucleic Acids Res. 47, D351-D360.

bioRxiv preprint doi: https://doi.org/10.1101/622266; this version posted April 29, 2019. The copyright holder for this preprint (which was not certified by peer review) is the author/funder, who has granted bioRxiv a license to display the preprint in perpetuity. It is made available under aCC-BY-NC-ND 4.0 International license.

48. Mohd, A.B., Palama, B., Nelson, S.E., Tomer, G., Nguyen, M., Huo, X., and Buermeyer, A.B. (2006). Truncation of the C-terminus of human MLH1 blocks intracellular stabilization of PMS2 and disrupts DNA mismatch repair. DNA Repair (Amst) 5, 347-361.

49. Moller, P., Seppala, T.T., Bernstein, I., Holinski-Feder, E., Sala, P., Gareth, E.D., Lindblom, A., Macrae, F., Blanco, I., Sijmons, R.H., Jeffries, J., Vasen, H.F.A., Burn, J., Nakken, S., Hovig, E., Rodland, E.A., Tharmaratnam, K., de Vos Tot Nederveen Cappel WH, Hill, J., Wijnen, J.T., Jenkins, M.A., Green, K., Lalloo, F., Sunde, L., Mints, M., Bertario, L., Pineda, M., Navarro, M., Morak, M., Renkonen-Sinisalo, L., Valentin, M.D., Frayling, I.M., Plazzer, J.P., Pylvanainen, K., Genuardi, M., Mecklin, J.P., Moeslein, G., Sampson, J.R., and Capella, G. (2018). Cancer risk and survival in path_MMR carriers by gene and gender up to 75 years of age: a report from the Prospective Lynch Syndrome Database. Gut 67, 1306-1316.

50. Nielsen, S.V., Poulsen, E.G., Rebula, C.A., and Hartmann-Petersen, R. (2014). Protein quality control in the nucleus. Biomolecules. 4, 646-661.

51. Nielsen, S.V., Stein, A., Dinitzen, A.B., Papaleo, E., Tatham, M.H., Poulsen, E.G., Kassem, M.M., Rasmussen, L.J., Lindorff-Larsen, K., and Hartmann-Petersen, R. (2017). Predicting the impact of Lynch syndrome-causing missense mutations from structural calculations. PLoS. Genet. 13, e1006739.

52. Olzmann, J.A., Brown, K., Wilkinson, K.D., Rees, H.D., Huai, Q., Ke, H., Levey, A.I., Li, L., and Chin, L.S. (2004). Familial Parkinson's disease-associated L166P mutation disrupts DJ-1 protein folding and function. J. Biol. Chem. 279, 8506-8515.

53. Palomaki, G.E., McClain, M.R., Melillo, S., Hampel, H.L., and Thibodeau, S.N. (2009). EGAPP supplementary evidence review: DNA testing strategies aimed at reducing morbidity and mortality from Lynch syndrome. Genet. Med. 11, 42-65.

54. Peltomaki, P. (2016). Update on Lynch syndrome genomics. Fam. Cancer 15, 385-393.

55. Peltomaki, P., Aaltonen, L.A., Sistonen, P., Pylkkanen, L., Mecklin, J.P., Jarvinen, H., Green, J.S., Jass, J.R., Weber, J.L., Leach, F.S., and . (1993). Genetic mapping of a locus predisposing to human colorectal cancer. Science 260, 810-812.

56. Peltomaki, P., and Vasen, H.F. (1997). Mutations predisposing to hereditary nonpolyposis colorectal cancer: database and results of a collaborative study. The International Collaborative Group on Hereditary Nonpolyposis Colorectal Cancer. Gastroenterology 113, 1146-1158.

57. Perera, S., and Bapat, B. (2008). The MLH1 variants p.Arg265Cys and p.Lys618Ala affect protein stability while p.Leu749Gln affects heterodimer formation. Hum. Mutat. 29, 332.

58. Pey, A.L., Stricher, F., Serrano, L., and Martinez, A. (2007). Predicted effects of missense mutations on native-state stability account for phenotypic outcome in phenylketonuria, a paradigm of misfolding diseases. Am. J. Hum. Genet. 81, 1006-1024.

59. Plaschke, J., Engel, C., Kruger, S., Holinski-Feder, E., Pagenstecher, C., Mangold, E., Moeslein, G., Schulmann, K., Gebert, J., von Knebel, D.M., Ruschoff, J., Loeffler, M., and Schackert, H.K. (2004). Lower incidence of colorectal cancer and later age of disease onset in 27 families with pathogenic MSH6 germline mutations compared with families with MLH1 or MSH2 mutations: the German Hereditary Nonpolyposis Colorectal Cancer Consortium. J. Clin. Oncol. 22, 4486-4494.

bioRxiv preprint doi: https://doi.org/10.1101/622266; this version posted April 29, 2019. The copyright holder for this preprint (which was not certified by peer review) is the author/funder, who has granted bioRxiv a license to display the preprint in perpetuity. It is made available under aCC-BY-NC-ND 4.0 International license.

60. Raevaara, T.E., Korhonen, M.K., Lohi, H., Hampel, H., Lynch, E., Lonnqvist, K.E., Holinski-Feder, E., Sutter, C., McKinnon, W., Duraisamy, S., Gerdes, A.M., Peltomaki, P., Kohonen-Ccorish, M., Mangold, E., Macrae, F., Greenblatt, M., de la Chapelle, A., and Nystrom, M. (2005). Functional significance and clinical phenotype of nontruncating mismatch repair variants of MLH1. Gastroenterology 129, 537-549.

61. Raschle, M., Dufner, P., Marra, G., and Jiricny, J. (2002). Mutations within the hMLH1 and hPMS2 subunits of the human MutLalpha mismatch repair factor affect its ATPase activity, but not its ability to interact with hMutSalpha. J. Biol. Chem. 277, 21810-21820.

62. Ravid, T., and Hochstrasser, M. (2008). Diversity of degradation signals in the ubiquitin-proteasome system. Nat. Rev. Mol. Cell Biol. 9, 679-690.

63. Rosenbaum, J.C., Fredrickson, E.K., Oeser, M.L., Garrett-Engele, C.M., Locke, M.N., Richardson, L.A., Nelson, Z.W., Hetrick, E.D., Milac, T.I., Gottschling, D.E., and Gardner, R.G. (2011). Disorder targets misorder in nuclear quality control degradation: a disordered ubiquitin ligase directly recognizes its misfolded substrates. Mol. Cell 41, 93-106.

64. Sachadyn, P. (2010). Conservation and diversity of MutS proteins. Mutat. Res. 694, 20-30.

65. Samant, R.S., Livingston, C.M., Sontag, E.M., and Frydman, J. (2018). Distinct proteostasis circuits cooperate in nuclear and cytoplasmic protein quality control. Nature 563, 407-411.

66. Scheller, R., Stein, A., Nielsen, S.V., Marin, F.I., Gerdes, A.M., Di, M.M., Papaleo, E., Lindorff-Larsen, K., and Hartmann-Petersen, R. (2019). Toward mechanistic models for genotype-phenotype correlations in phenylketonuria using protein stability calculations. Hum. Mutat. 40, 444-457.

67. Schymkowitz, J., Borg, J., Stricher, F., Nys, R., Rousseau, F., and Serrano, L. (2005). The FoldX web server: an online force field. Nucleic Acids Res. 33, W382-W388.

68. Shimodaira, H., Filosi, N., Shibata, H., Suzuki, T., Radice, P., Kanamaru, R., Friend, S.H., Kolodner, R.D., and Ishioka, C. (1998). Functional analysis of human MLH1 mutations in Saccharomyces cerevisiae. Nat. Genet. 19, 384-389.

69. Sijmons, R.H., and Hofstra, R.M. (2016). Review: Clinical aspects of hereditary DNA Mismatch repair gene mutations. DNA Repair (Amst) 38, 155-162.

70. Stein, A., Fowler, D.M., Hartmann-Petersen, R., and Lindorff-Larsen, K. (2019). Biophysical and Mechanistic Models for Disease-Causing Protein Variants. Trends Biochem. Sci.

71. Takahashi, M., Shimodaira, H., Andreutti-Zaugg, C., Iggo, R., Kolodner, R.D., and Ishioka, C. (2007). Functional analysis of human MLH1 variants using yeast and in vitro mismatch repair assays. Cancer Res. 67, 4595-4604.

72. Thompson, B.A., Spurdle, A.B., Plazzer, J.P., Greenblatt, M.S., Akagi, K., Al-Mulla, F., Bapat, B., Bernstein, I., Capella, G., den Dunnen, J.T., du, S.D., Fabre, A., Farrell, M.P., Farrington, S.M., Frayling, I.M., Frebourg, T., Goldgar, D.E., Heinen, C.D., Holinski-Feder, E., Kohonen-Corish, M., Robinson, K.L., Leung, S.Y., Martins, A., Moller, P., Morak, M., Nystrom, M., Peltomaki, P., Pineda, M., Qi, M., Ramesar, R., Rasmussen, L.J., Royer-Pokora, B., Scott, R.J., Sijmons, R., Tavtigian, S.V., Tops, C.M., Weber, T., Wijnen, J., Woods, M.O., Macrae, F., and Genuardi, M. (2014). Application of a 5-tiered scheme for standardized classification

bioRxiv preprint doi: https://doi.org/10.1101/622266; this version posted April 29, 2019. The copyright holder for this preprint (which was not certified by peer review) is the author/funder, who has granted bioRxiv a license to display the preprint in perpetuity. It is made available under aCC-BY-NC-ND 4.0 International license.

of 2,360 unique mismatch repair gene variants in the InSiGHT locus-specific database. Nat. Genet. 46, 107-115.

73. Tokuriki, N., and Tawfik, D.S. (2009). Stability effects of mutations and protein evolvability. Curr. Opin. Struct. Biol. 19, 596-604.

74. Tomer, G., Buermeyer, A.B., Nguyen, M.M., and Liskay, R.M. (2002). Contribution of human mlh1 and pms2 ATPase activities to DNA mismatch repair. J. Biol. Chem. 277, 21801-21809.

75. van der Lee, R., Lang, B., Kruse, K., Gsponer, J., Sanchez de, G.N., Huynen, M.A., Matouschek, A., Fuxreiter, M., and Babu, M.M. (2014). Intrinsically disordered segments affect protein half-life in the cell and during evolution. Cell Rep. 8, 1832-1844.

76. Vasen, H.F., and de Vos Tot Nederveen Cappel WH. (2013). A hundred years of Lynch syndrome research (1913-2013). Fam. Cancer 12, 141-142.

77. Vasen, H.F., Wijnen, J.T., Menko, F.H., Kleibeuker, J.H., Taal, B.G., Griffioen, G., Nagengast, F.M., Meijers-Heijboer, E.H., Bertario, L., Varesco, L., Bisgaard, M.L., Mohr, J., Fodde, R., and Khan, P.M. (1996). Cancer risk in families with hereditary nonpolyposis colorectal cancer diagnosed by mutation analysis. Gastroenterology 110, 1020-1027.

78. Wagih, O., Galardini, M., Busby, B.P., Memon, D., Typas, A., and Beltrao, P. (2018). A resource of variant effect predictions of single nucleotide variants in model organisms. Mol. Syst. Biol. 14, e8430.

79. Wu, H., Zeng, H., Lam, R., Tempel, W., Kerr, I.D., and Min, J. (2015). Structure of the human MLH1 N-terminus: implications for predisposition to Lynch syndrome. Acta Crystallogr. F. Struct. Biol. Commun. 71, 981-985.

80. Wu, X., Platt, J.L., and Cascalho, M. (2003). Dimerization of MLH1 and PMS2 limits nuclear localization of MutLalpha. Mol. Cell Biol. 23, 3320-3328.

81. Yanagitani, K., Juszkiewicz, S., and Hegde, R.S. (2017). UBE2O is a quality control factor for orphans of multiprotein complexes. Science 357, 472-475.

82. Zimmermann, L., Stephens, A., Nam, S.Z., Rau, D., Kubler, J., Lozajic, M., Gabler, F., Soding, J., Lupas, A.N., and Alva, V. (2018). A Completely Reimplemented MPI Bioinformatics Toolkit with a New HHpred Server at its Core. J. Mol. Biol. 430, 2237-2243.

bioRxiv preprint doi: https://doi.org/10.1101/622266; this version posted April 29, 2019. The copyright holder for this preprint (which was not certified by peer review) is the author/funder, who has granted bioRxiv a license to display the preprint in perpetuity. It is made available under aCC-BY-NC-ND 4.0 International license.

Figure legends

Figure 1. MLH1 structural stability predictions. (A) Structure of MLH1 (PDB IDs 4P7A and 3RBN). Positions of variants tested in this work are highlighted with coloured spheres, indicating the predicted ΔΔG (<0.5 kcal/mol, purple, <1, cyan, <3.5 green, <7, yellow, <12, orange, >12, red). (B) Many disease-linked MLH1 missense variants (red) are structurally destabilized and therefore, compared to wild-type MLH1 (green), more likely to unfold. (C) The free energy of the folded conformation of a destabilized missense variant (red) is closer to that of the fully unfolded state. The employed stability calculations predict the difference of the free energy (ΔΔG) between a missense variant (red) and wild-type MLH1 (green). (D) Excerpt of the *in silico* saturation mutagenesis map (full dataset provided in supplemental material file 1). (E) Distribution of all predicted ΔΔGs from saturation mutagenesis. The peak at 15 kcal/mol contains all variants with ΔΔG values greater than this value.

Figure 2. Steady-state levels of MLH1 variants correlate with structural stability predictions. (A) Example of the immunofluorescence imaging of HCT116 cells using antibodies to MLH1. Hoechst staining was used to mark the nucleus. Note the reduced steady-state levels of the G67R MLH1 variant compared to wild-type MLH1. (B) The total fluorescent intensity for each of the 69 different MLH1 variants was determined after excluding the non-transfected cells and normalizing the intensities to that for wild-type MLH1. The intensities were then plotted vs. the predicted ΔΔG values. Between 200 and 1,000 cells were included for each quantification. The error bars indicate the standard error of the mean (n = 5 experiments). Each variant is color-coded according to the ClinVar disease category. (C) Distribution of steady-state levels by DME category – 0 is loss-of-function in all assays by Takahashi *et al.* (Takahashi et al., 2007), 3 represents function in all these assays (for details see the Materials and Methods). Raincloud plot visualization as described in (Allen et al., 2018) Gray dots represent means within each DME category, with bars for standard error. (D) Distribution of FoldX ΔΔGs across DME categories (as in (C)). (E) FoldX ΔΔGs for all variants tested in this work, indicating their position in the MLH1 sequence. As elsewhere, values above 15 kcal/mol were here set to this value.

Figure 3. Many MLH1 variants are degraded by the proteasome. (A) HCT116 cells transfected with the indicated MLH1 variants were analyzed by blotting with antibodies to MLH1. Co-transfection with a plasmid expressing GFP was included to test the transfection efficiencies between the MLH1 variants. β-actin served as a loading control. (B) Quantification of blots as in (A) normalized to the steady-state level of wild-type (WT) MLH1. The error bars show the standard deviation (n=3). (C) MLH1-transfected HCT116 cells were treated with 25 μg/mL cycloheximide (CHX) for 0, 4, 8 or 12 hours, and lysates were analyzed by blotting using antibodies to MLH1. β-actin was used as a loading control. (D) Quantification of blots as in panel (C), normalized to the steady-state levels at t = 0 hours. The error bars indicate the standard deviation (n=3). (E) Western blotting with antibodies to MLH1 of whole cell lysates from transfected cells either untreated or treated for 16 hours with 10 μM bortezomib (BZ). Blotting for β-actin was included as a loading

bioRxiv preprint doi: https://doi.org/10.1101/622266; this version posted April 29, 2019. The copyright holder for this preprint (which was not certified by peer review) is the author/funder, who has granted bioRxiv a license to display the preprint in perpetuity. It is made available under aCC-BY-NC-ND 4.0 International license.

control. (F) Quantification of blots as in panel (E) normalized to steady-state levels after BZ treatment. The error bars indicate the standard deviation (n=3).

Figure 4. Stable MLH1 variants increase steady-state levels of PMS1 and PMS2. (A) The levels of endogenous PMS1 and PMS2 were determined by blotting of whole-cell lysates of HCT116 cells transfected with either empty vector or with wild-type MLH1 and treated with 25 µg/mL cycloheximide (CHX) for 0, 4, 8 or 12 hours. The antibodies used were to PMS1 and PMS2, and as a control to MLH1. β-actin served as loading control. (B) Quantification of blots as in panel (A) normalized to protein levels at 0 hours. The error bars indicate the standard deviation (n=3). (C) The levels of endogenous MLH1, PMS1 and PMS2 were compared by blotting of cell lysates of HCT116 cells either untreated, or treated with cycloheximide (CHX) or with bortezomib (BZ) and CHX. β-actin served as loading control. (D) The levels of endogenous PMS1 and PMS2 and transfected MLH1 were compared by Western blotting using antibodies to PMS1, PMS2 and MLH1. β-actin served as loading control. (E) Quantification of blots as in panel (C) normalized to the level of endogenous PMS1 or PMS2 in untransfected HCT116 cells. The error bars show the standard deviation (n=3). (F) Plotting the levels of the MLH1 variants vs. the levels of endogenous PMS1 and PMS2. The error bars show the standard deviation (n=3). (G) The levels of MLH1 and YFP-tagged PMS2 were analyzed by SDS-PAGE and blotting of whole-cell lysates of HCT116 cells transfected with the indicated expression plasmids. β-actin was included as loading control. (H) Co-transfected PMS2-YFP was immunoprecipitated (IP) using GFP-trap beads, and the precipitated material was analyzed by electrophoresis and blotting. Bortezomib was added to all cultures 16 hours prior to cell lysis to ensure ample amounts of the unstable MLH1 variants.

Figure 5. Molecular chaperones play a role in the proteasomal degradation of MLH1. (A) Co-transfected HSP70-myc was immunoprecipitated (IP) using myc-trap beads and analyzed by blotting with antibodies to the myc-tag (HSP70) and MLH1. Bortezomib was added to all cultures 8 hours prior to cell lysis to ensure ample amounts of the unstable MLH1 variants. (B) Quantification of blots as shown in panel (A) normalized to level of wild-type MLH1. The error bars indicate the standard deviation (n=3). (C) Co-transfected HSP90-HA was immunoprecipitated (IP) with anti-HA resin, and the precipitated material analyzed by electrophoresis and Western blotting using antibodies to the HA-tag (HSP90) and MLH1. As above, bortezomib was added to all cultures prior to cell lysis. (D) Quantification of blots as in panel (C) normalized to amount of precipitated wild-type MLH1. The error bars show the standard deviation (n=3). (E) Western blotting using antibodies to MLH1 of whole-cell lysates from transfected cells treated with 5 µM YM01 for 24 hours as indicated. (F) Western blotting using antibodies to MLH1 of whole-cell lysates from transfected cells treated 1 µM geldanamycin (GA) for 24 hours.

Figure 6. Assessing stability calculations for predicting pathogenicity. (A) Plot of ΔΔG-values vs. allele frequencies for all variants listed in gnomAD (gray), as well as those analyzed by Takahashi *et al.*; the latter are color-coded by DME. Note that the leftmost group of colored dots are variants that have been reported in patients, but are not recorded in gnomAD (thus their allele frequency in gnomAD is zero). Variants with common to intermediate frequencies are all predicted to be stable,

bioRxiv preprint doi: https://doi.org/10.1101/622266; this version posted April 29, 2019. The copyright holder for this preprint (which was not certified by peer review) is the author/funder, who has granted bioRxiv a license to display the preprint in perpetuity. It is made available under aCC-BY-NC-ND 4.0 International license.

while some rare variants are predicted to be destabilized. (B) FoldX ΔΔG for benign (blue), likely benign (cyan), likely pathogenic (orange), and pathogenic (red) variants that are reported in ClinVar with "at least one star" curation. (C) Evolutionary sequence energies for ClinVar-reported variants, color scheme as in (B). (D) ROC curves for FoldX ΔΔGs, evolutionary sequence energies, and sequence-based predictors (PolyPhen2, PROVEAN) to assess their performance in separating benign from pathogenic variants. As there are 16 benign and 66 pathogenic MLH1 missense variants in ClinVar, we split the pathogenic variants into 4 sets, performed ROC analysis of each subset to the benign variants, and report the average ROC curves and area under the curves (AUCs) here. TPR, true positive rate. FPR, false positive rate. (E) Landscape of variant tolerance by combination of changes in protein stability (x axis) and evolutionary sequence energies (y axis), such that the upper right corner indicates most likely detrimental variants, while those in the lower left corner are predicted stable and observed in MLH1 homologs. The green background density illustrates the distribution of all variants listed in gnomAD. The combination of metrics captures most non-functional variants (DME scores 0 or 1). Outliers are discussed in the main text.

Figure 7. Model for how structural destabilization of MLH1 contributes to disease. The wild-type (green) MLH1-PMS2 heterodimer promotes DNA mismatch repair. Disease-linked missense MLH1 variants (red) may also promote DNA repair, but are at risk of dissociating from PMS2 due to structural destabilization. The structural destabilization of MLH1 may also cause a partial unfolding of MLH1 which is recognized by the molecular chaperone HSP70 and causes proteasomal degradation of the MLH1 variant. In turn, the degradation of MLH1 leaves PMS2 without a partner protein, resulting in proteasomal degradation of PMS2.

bioRxiv preprint doi: https://doi.org/10.1101/622266; this version posted April 29, 2019. The copyright holder for this preprint (which was not certified by peer review) is the author/funder, who has granted bioRxiv a license to display the preprint in perpetuity. It is made available under aCC-BY-NC-ND 4.0 International license.

Figure 1

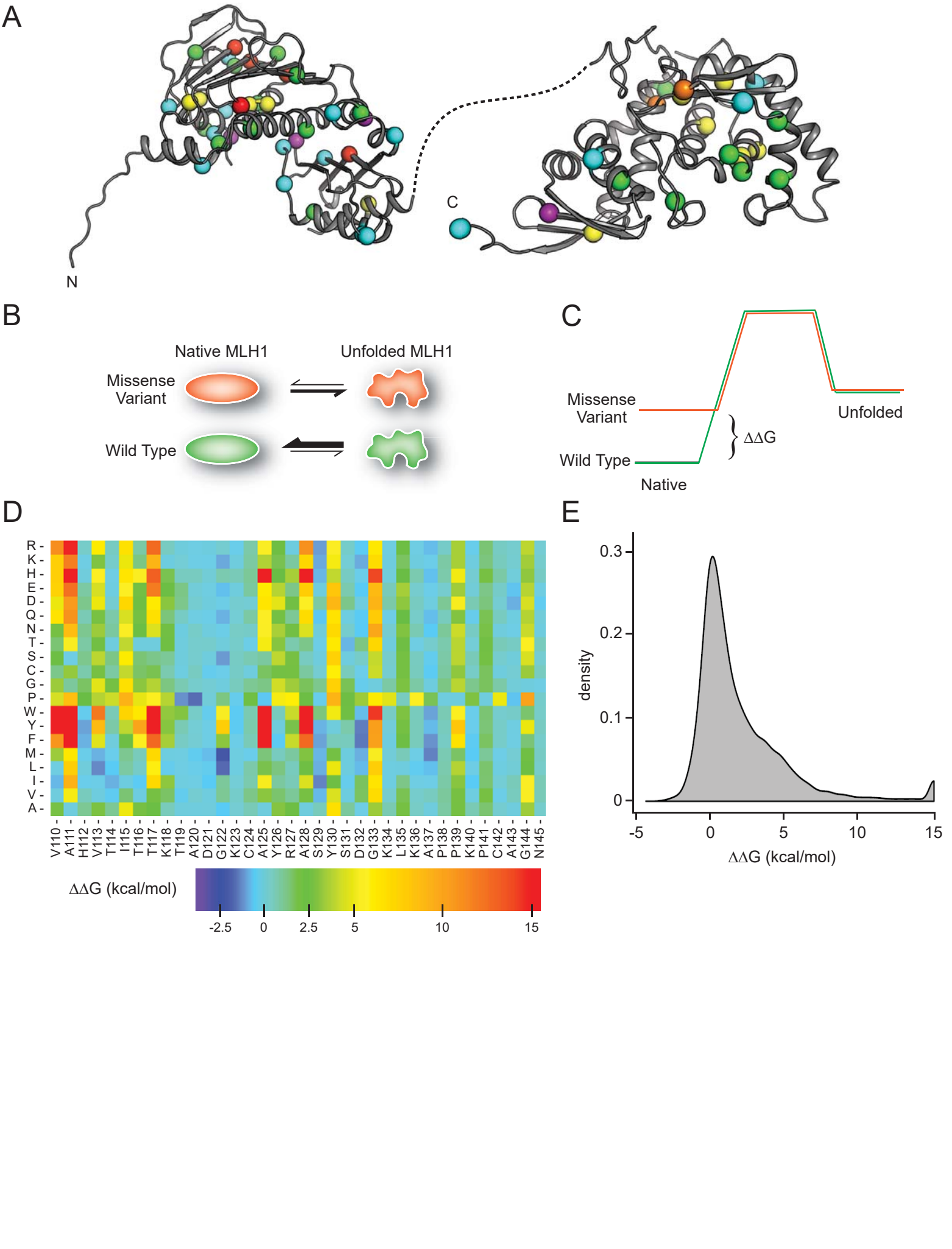

bioRxiv preprint doi: https://doi.org/10.1101/622266; this version posted April 29, 2019. The copyright holder for this preprint (which was not certified by peer review) is the author/funder, who has granted bioRxiv a license to display the preprint in perpetuity. It is made available under aCC-BY-NC-ND 4.0 International license.

Figure 2

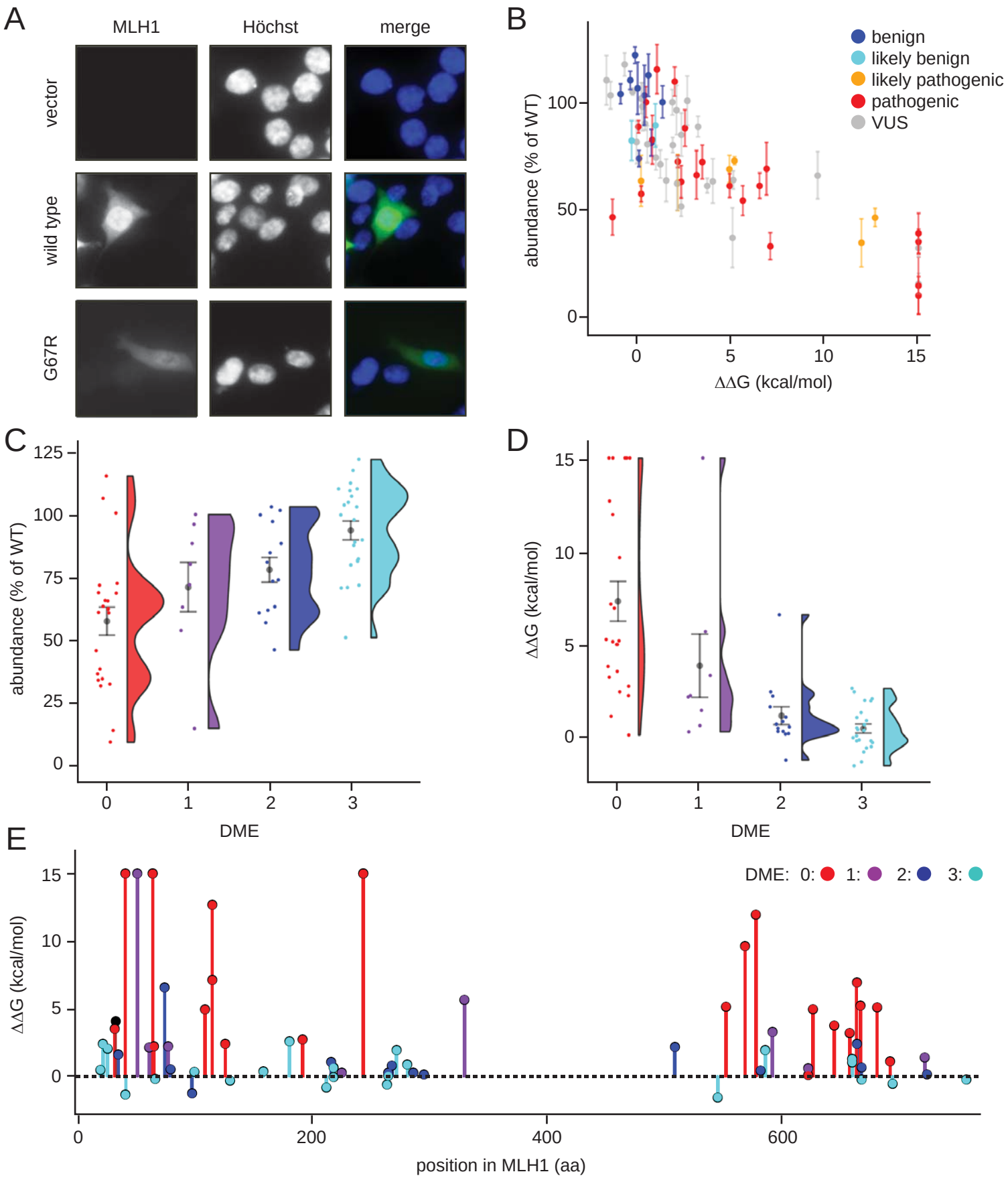

bioRxiv preprint doi: https://doi.org/10.1101/622266; this version posted April 29, 2019. The copyright holder for this preprint (which was not certified by peer review) is the author/funder, who has granted bioRxiv a license to display the preprint in perpetuity. It is made available under aCC-BY-NC-ND 4.0 International license.

Figure 3

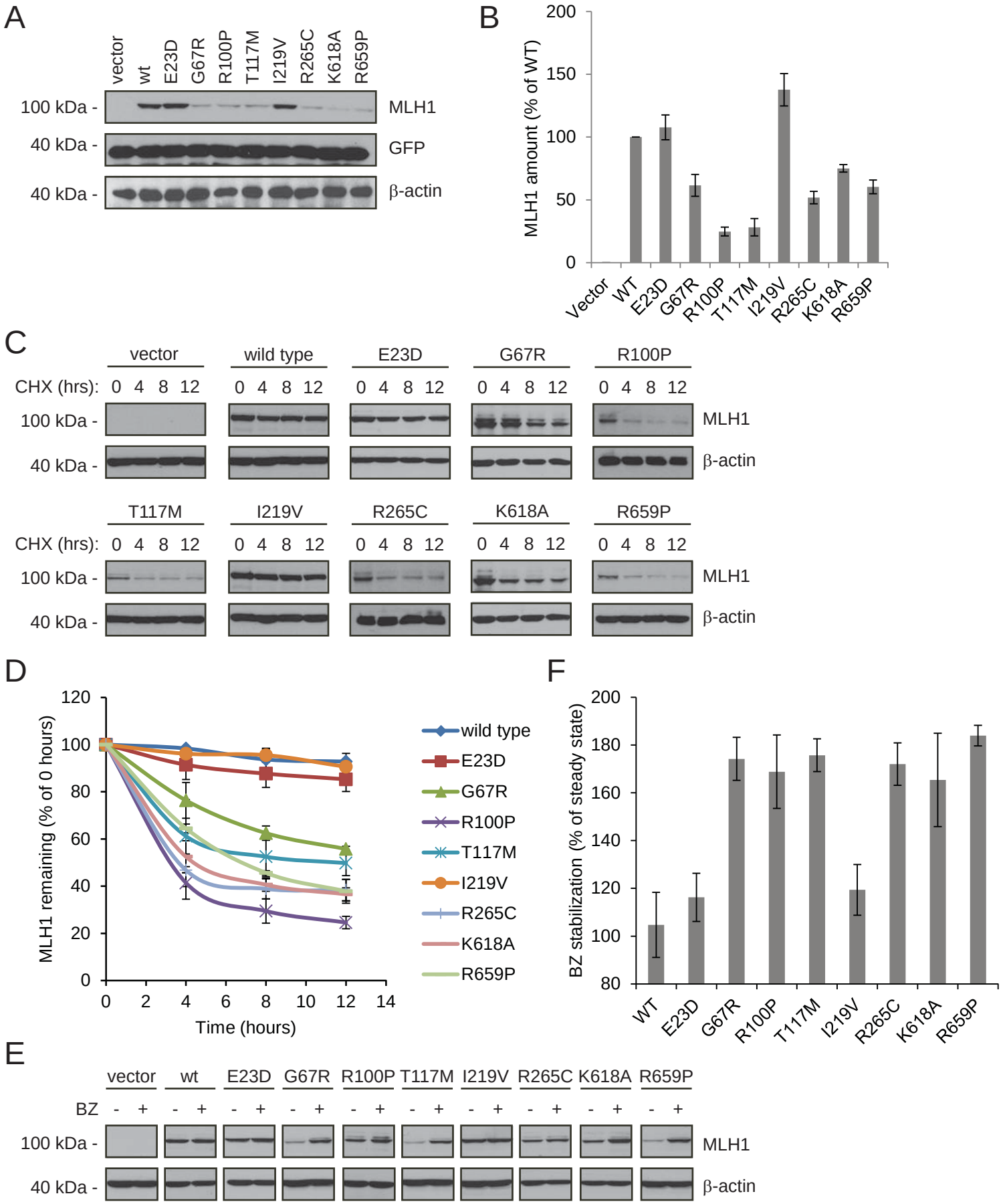

bioRxiv preprint doi: https://doi.org/10.1101/622266; this version posted April 29, 2019. The copyright holder for this preprint (which was not certified by peer review) is the author/funder, who has granted bioRxiv a license to display the preprint in perpetuity. It is made available under aCC-BY-NC-ND 4.0 International license.

Figure 4

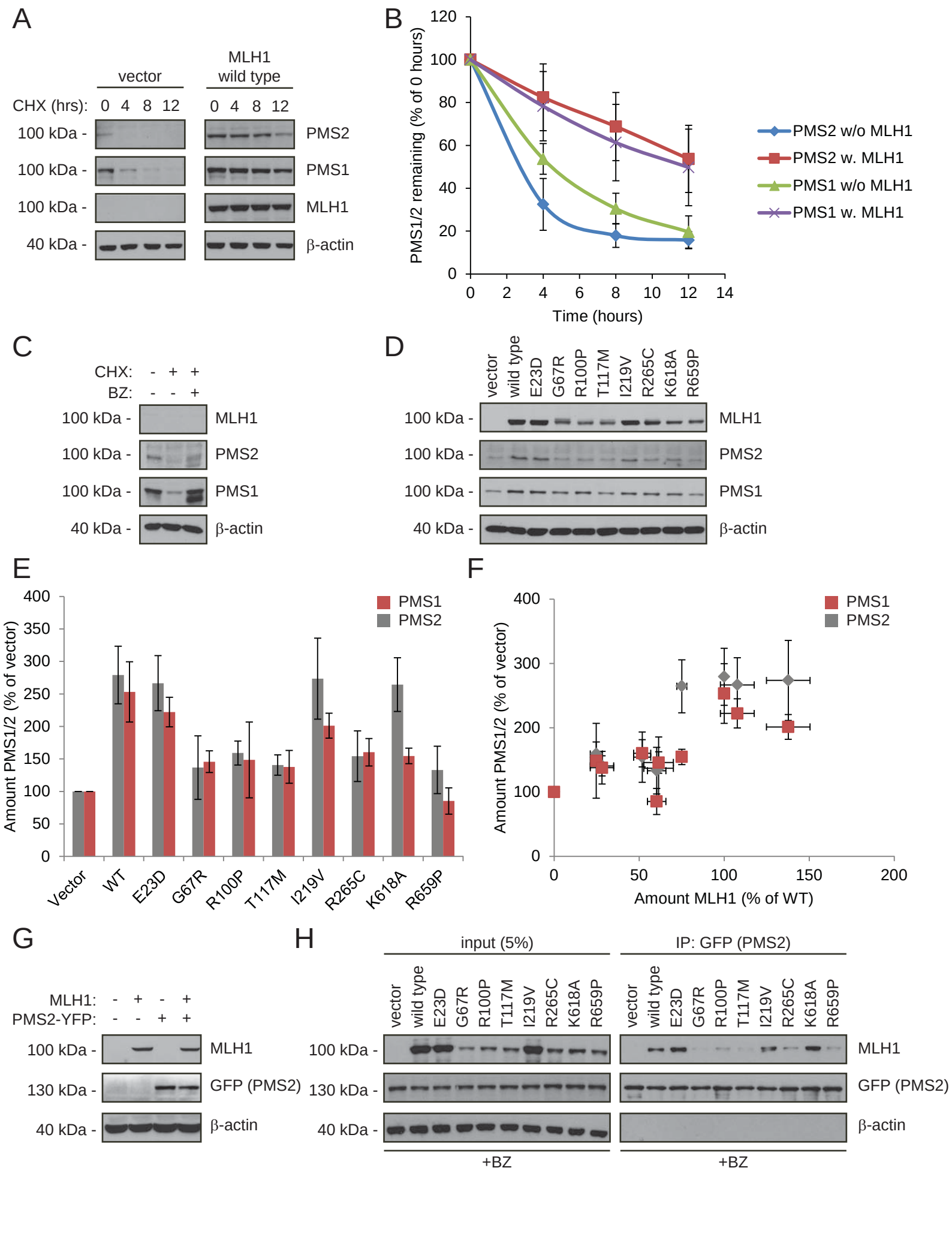

bioRxiv preprint doi: https://doi.org/10.1101/622266; this version posted April 29, 2019. The copyright holder for this preprint (which was not certified by peer review) is the author/funder, who has granted bioRxiv a license to display the preprint in perpetuity. It is made available under aCC-BY-NC-ND 4.0 International license.

Figure 5

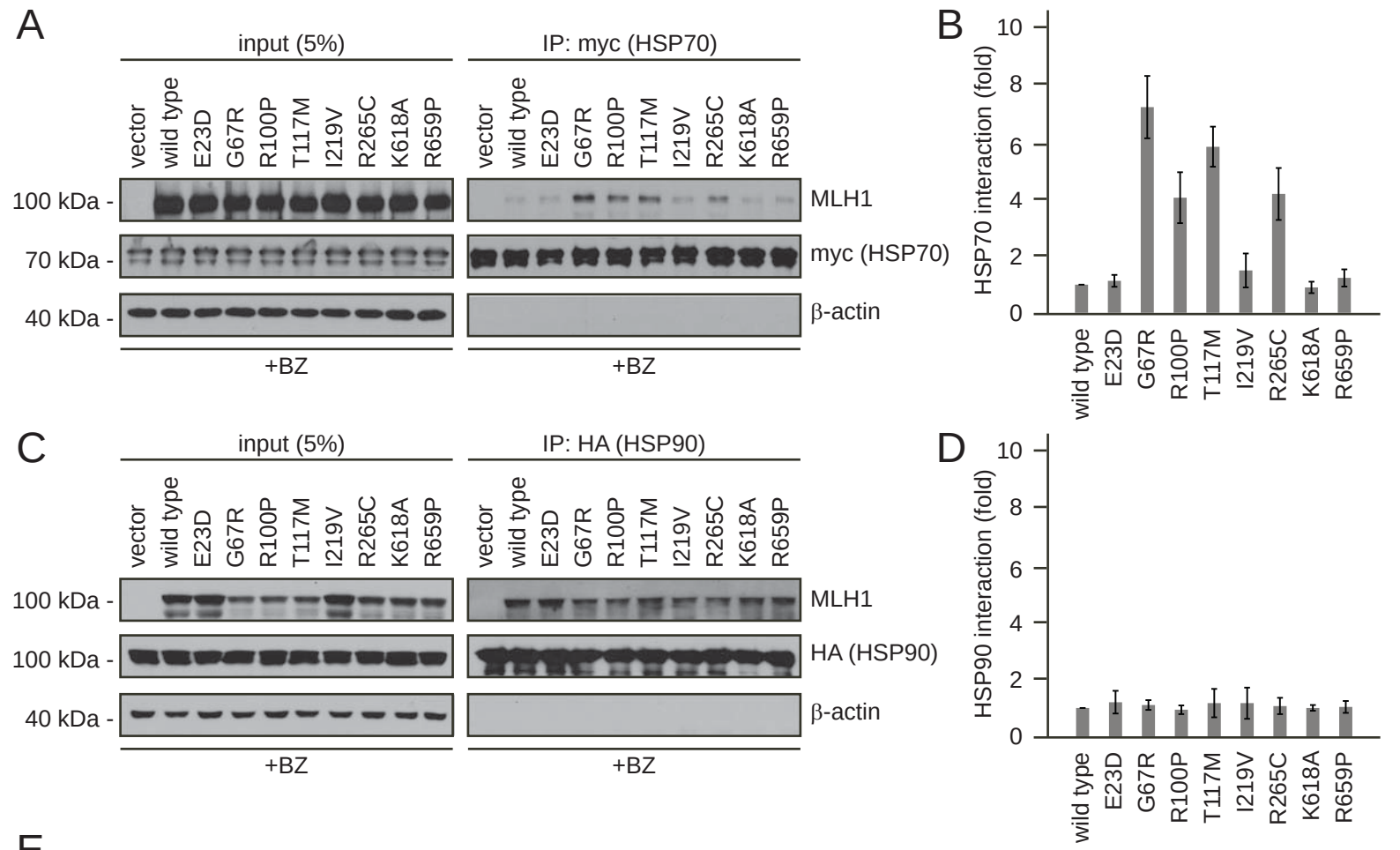

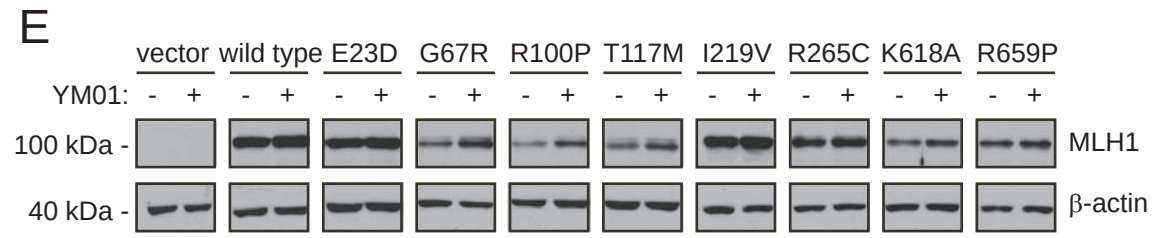

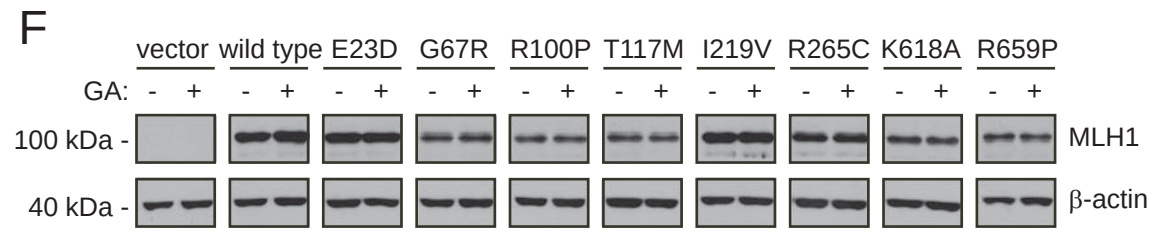

bioRxiv preprint doi: https://doi.org/10.1101/622266; this version posted April 29, 2019. The copyright holder for this preprint (which was not certified by peer review) is the author/funder, who has granted bioRxiv a license to display the preprint in perpetuity. It is made available under aCC-BY-NC-ND 4.0 International license.

Figure 6

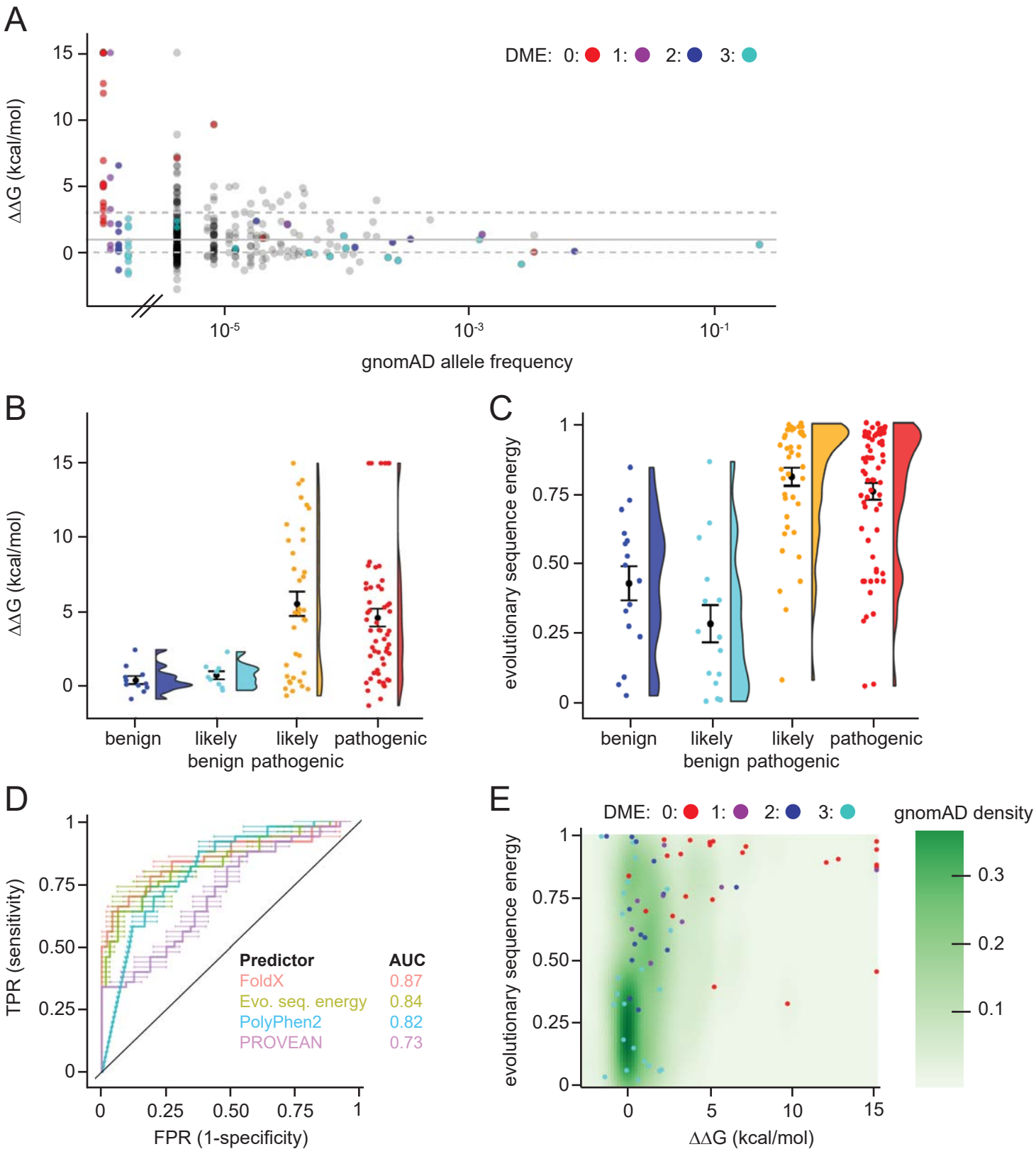

bioRxiv preprint doi: https://doi.org/10.1101/622266; this version posted April 29, 2019. The copyright holder for this preprint (which was not certified by peer review) is the author/funder, who has granted bioRxiv a license to display the preprint in perpetuity. It is made available under aCC-BY-NC-ND 4.0 International license.

Figure 7